Variable tree rooting strategies are key to model distribution, productivity and evapotranspiration of tropical evergreen forests

Boris Sakschewski[1], Werner von Bloh[1], Markus Drüke[1], Anna A. Sörensson[2, 3], Romina Ruscica[2, 3], Fanny Langerwisch[4, 5], Maik Billing[1], Sarah Bereswill[6], Marina Hirota[7, 8], Rafael S. Oliveira[8], Jens Heinke[1], Kirsten Thonicke[1]

[1]Potsdam Institute for Climate Impact Research, Potsdam, 14473, Germany
[2]Universidad de Buenos Aires - Consejo Nacional de Investigaciones Científicas y Técnicas, Centro de Investigaciones del Mar y la Atmósfera (CIMA/UBA-CONICET), Buenos Aires, Argentina.
[3]Institut Franco-Argentin d'Etudes sur le Climat et ses Impacts, Unité Mixte Internationale (UMI-IFAECI/CNRS-CONICET-UBA), Argentina
[4]Czech University of Life Sciences Prague, Department of Water Resources and Environmental Modeling, 165 00 Praha 6 – Suchdol, Czech Republic
[5]Palacký University Olomouc, Department of Ecology and Environmental Sciences, 78371 Olomouc, Czech Republic
[6]University of Potsdam, Potsdam, 14469, Germany
[7]Federal University of Santa Catarina (UFSC), Campus Universitário Reitor João David Ferreira Lima Trindade – Florianópolis – SC, CEP: 88040-900, Santa Catarina, Brazil
[8]University of Campinas (UNICAMP) Cidade Universitária "Zeferino Vaz" CEP 13083-970, Campinas-SP, Sao Paulo, Brazil

Correspondence to: Boris Sakschewski (boris.sakschewski@pik-potsdam.de)

Abstract. A variety of modelling studies have suggested tree rooting depth as a key variable to explain evapotranspiration rates, productivity and the geographical distribution of evergreen forests in tropical South America. However, none of those studies acknowledged resource investment, timing and physical constraints of tree rooting depth within a competitive environment, undermining the ecological realism of their results. Here we present an approach of implementing variable rooting strategies and dynamic root growth into the LPJmL4.0 DGVM and apply it to tropical and sub-tropical South-America under contemporary climate conditions. We show how competing rooting strategies which underlie the trade-off between above- and below-ground carbon investment lead to more realistically simulated intra-annual productivity and evapotranspiration, and consequently forest cover and spatial biomass distribution. We find that climate and soil depth determine a spatially heterogeneous pattern of mean rooting depth and belowground biomass across the study region. We conclude that the ability of evergreen trees to adjust their rooting systems to seasonally dry climates is crucial to explain the current dominance, productivity and evapotranspiration of evergreen forests in tropical South America.

1 Introduction

Tropical evergreen forest is the naturally dominant biome type in South-America over a large climatic range including regions with a marked dry season (Hirota et al., 2011; Xiao et al., 2006). To withstand seasonal shortages of precipitation and sustain productivity, trees with evergreen phenology often gain access to deep soil water via deep roots (Brum et al., 2019; Canadell et al., 1996; Johnson et al., 2018; Kim et al., 2012; Markewitz et al., 2010). Consequently, recent studies suggest a heterogeneous spatial pattern of maximum rooting depth across tropical forest biomes in South-America which differs over the order of magnitudes depending on local groundwater, soil and climate conditions (Canadell et al., 1996; Fan et al., 2017). Therefore, tree rooting depth is regarded as a crucial variable to explain the geographical distribution of main phenology strategies such as evergreen and deciduous, as well as the observed local to continental pattern of productivity, biomass storage, evapotranspiration (ET) and consequently moisture recycling (Fan et al., 2017; Jobbágy and Jackson, 2000; Kleidon and Heimann, 2000; Langan et al., 2017; Nepstad et al., 1994; Stahl et al., 2013). While these variables and processes are in the focus of model-based earth system sciences projecting the development of vegetation formation and ecosystem functioning worldwide (Huntingford et al., 2013; Liu et al., 2018; Weber et al., 2009), most DGVMs and land-surface models (LSMs) still do not represent the diversity of rooting depth or tree rooting strategies (Warren et al., 2015a). In general these models condense the diversity of such functional tree traits into so called plant functional types (PFTs), which

represent average tree growing strategies on scales as large as biomes. Here, often a shallow rooting depth for tree PFTs is assumed, i.e. most roots are distributed downwards to a few meters of depths at maximum (Arora and Boer, 2003; Best et al., 2011; Guimberteau et al., 2017; Lawrence et al., 2011; Ostle et al., 2009; Schaphoff et al., 2018; Smith et al., 2014).

By ignoring natural local adaptations of rooting depth, DGVMs and LSMs in the past had problems reproducing the extent of South-America's tropical evergreen forests, as well as its seasonal productivity and ET especially in regions with seasonal rainfall (Baudena et al., 2014; Liu et al., 2018, 2017; Restrepo-Coupe et al., 2017). So far different approaches were presented trying to solve this problem in DGVMs and similar models by allowing for variable rooting strategies. In a pioneering study more than 20 years ago, Kleidon and Heimann (1998) systematically searched for rooting strategies which yield highest net primary productivity over South America in a DGVM to explain intra-annual rates of ET and vegetation cover. Follow up studies further underlined the importance of deep roots for the climate system of South America (Kleidon and Heimann, 2000). Lee *et al.* (2005) found that allowing for deep roots and hydraulic redistribution of water in the soil column in a general circulation model enhances Amazon forest productivity and evapotranspiration (ET) in the dry season. Baker *et al.* (2008) came to similar results when introducing deep roots in a land surface model. Ichii *et al.*, (2007) found that constraining rooting depth across the Amazon based on satellite data yields similar results in a terrestrial ecosystem model. More recently, Langan, Higgins and Scheiter (2017) showed for the same study area how diverse rooting strategies in a tree individual and trait-based DGVM can improve simulated intra-annual productivity and ET and better explain patterns of different tropical biome types and biomass in connection with fire.

While these studies are important steps to acknowledge the diversity of tree rooting strategies and its effects, some assumptions of the underlying models might decrease the liability of their results. These assumptions are related to 1) resource investment, 2) timing and 3) physical constraints of rooting depth. 1) Most models so far do not account for coarse roots (Warren et al., 2015a) even though they can make up the majority of total root biomass (Xiao et al., 2003). This approach may be sufficient when employing shallow tree rooting strategies only, but with increasing rooting depth, costs for coarse roots increases substantially. Since the amount of resources trees can allocate to their processes and structures is finite, a local adaptation of tree rooting depth must follow a trade-off between above- and below-ground resource investment (Nikolova et al., 2011). Generally above-ground investments into leaf and stem growth can increase light absorption and CO_2 uptake, while below-ground investments can increase the uptake of water and nutrients. Depending on local environmental and competitive conditions one or the other allocation strategy might be more advantageous, eventually leading to substantial regional variation in the mean below-ground to above-ground biomass ratios (Leuschner et al., 2007; Mokany et al., 2006). Therefore, the simulated spectrum of tree rooting strategies which can survive and co-exist should be in accordance with this crucial trade-off. 2) In contrast to above-ground stem growth, most DGVMs so far do not simulate gradual root growth (Warren et al., 2015a). Instead PFTs are assigned a constant relative distribution of fine roots throughout the soil column at any point in space and time (Best et al., 2011; Lawrence et al., 2011; Schaphoff et al., 2018; Smith et al., 2014). As under the above mentioned simplification under 1), this approach may be sufficient when accounting for shallow rooting strategies only, but when the maximum tree rooting depth of PFTs strongly diverges, it is questionable that the time needed to reach this depth is negligible, especially when accounting for PFT competition. Rooting depth increases rather gradually and non-linear over a tree's lifetime with a velocity driven by a mix of plastic optimization and allometric determination (Brum et al., 2019; Brunner et al., 2015; Nikolova et al., 2011; Poorter et al., 2012; Warren et al., 2015b). Even though non-DGVM related models have implemented root optimization schemes in the past (Schymanski et al., 2008), the knowledge base for a mechanistic bottom-up modelling approach of plastic root optimization is very sparse (Jenik, 2010; Poorter et al., 2012; Warren et al., 2015b) and knowledge on certain allometric rules (Brum et al., 2019; Eshel and Grünzweig, 2013; Mokany et al., 2006) seems enough to be applied in DGVMs. 3) Most DGVMs so far do not account for a location-dependent soil depth, but apply a constant soil depth across the globe (Best et al., 2011; Guimberteau et al., 2017; Lawrence et al., 2011; Ostle et al., 2009; Schaphoff et al., 2018; Smith et al., 2014). Again this approach may be sufficient

90 when accounting for shallow rooting strategies only, but allowing for deep tree rooting strategies should go in parallel with

91 their potential physical barriers. Recent data products on global soil depth now enable to better constrain rooting depth in

92 DGVMs (Pelletier et al., 2016).

93 Here we overcome the above mentioned limitations and present a new approach of diversifying tree rooting strategies in the

94 DGVM LPJmL4.0 (Lund-Potsdam-Jena managed Lands; Schaphoff *et al.*, 2018) which increases the ecological liability

95 with the following aspects: 1) Maximum rooting depth is restricted to a recent global product of soil depth, 2) simulated tree

96 rooting strategies were chosen to represent a wide range of maximum rooting depth between 0.5 and 18 m, 3) all tree rooting

97 strategies of this spectrum grow in competition and PFT performance determines dominance, 4) dominance is supported by

98 best performing rooting strategies increasing their establishment rate, 5) PFTs have to invest into coarse roots as well, i.e.

99 acknowledging the trade-off between growing deeper roots and allocating available carbon to other compartments (stem and

100 leaf growth), and 6) tree PFT roots are growing deeper over time depending on tree height.

101 Given these new model developments we here re-evaluate the hypothesis that varying tree rooting depth is key to explain

102 major patterns of evapotranspiration, productivity and the geographical distribution of tropical evergreen forests in South

103 America, as we acknowledge a diversity of different competing tree rooting strategies as well as resource investment, timing

104 and physical constraints of rooting depth. Therefore, we compare several model versions of LPJmL4.0 differing in the above

105 mentioned model developments and evaluate simulated evapotranspiration, productivity, biomass and spatial distribution of

106 evergreen and deciduous tree PFTs using different sources of validation data.

2 Materials and Methods

2.1 The LPJmL4.0 model

109 LPJmL4.0 is a process-based Dynamic Global Vegetation Model (DGVM) which simulates the surface energy balance,

110 water fluxes, fire disturbance, carbon fluxes and stocks of the global land (Schaphoff et al., 2018). Plant productivity is

111 modelled on the basis of leaf-level photosynthesis responding to climatic and environmental conditions, atmospheric CO_2

112 concentration, canopy conductance, autotrophic respiration, phenology and management intensity. Fire disturbance is

113 modelled using the simple fire module Glob-FIRM (Thonicke et al., 2001) which relates the length of the fire season to

114 fractional annual area burnt. The model simulates 11 plant functional types (PFTs), 3 bioenergy functional types (BFTs) and

115 12 crop functional types (CFTs), to represent average plants of natural vegetation, bioenergy plantations and agriculture,

116 respectively. Three PFTs represent the natural vegetation of the tropics and sub-tropics namely the "tropical broadleaved

117 evergreen tree" mainly representing tropical evergreen forest, the "tropical broadleaved deciduous tree" representing tropical

118 dry forest and the woody component of savanna and "tropical herbs" representing the herbaceous layer in grasslands,

119 savanna and forests.

120 The standard spatial model resolution is a 0.5° x 0.5° longitude-latitude grid. For each grid cell the fractional coverage of

121 bioenergy and agricultural BFTs and CFTs follows a prescribed land-use data set, whereas in the remaining grid-cell area

122 natural PFTs grow in competition.

2.2 A new tree rooting scheme for LPJmL4.0

124 In this section we describe the new basic scheme for soil layer partitioning, the new tree rooting scheme, the simulation of

125 belowground carbon investment, and how different tree rooting strategies (implemented in the new scheme) compete. All

126 changes made to LPJmL4.0 described in this section result in a new sub-version of LPJmL4.0 which we call LPJmL4.0-VR

127 hereafter (where "VR" stands for variable roots).

2.2.1 Scheme for soil layer partitioning

LPJmL4.0 employs a globally universal soil depth of 3 m. For LPJmL4.0-VR we extended the general maximum soil depth to 20 m (but restrict it to local soil depth information at spatial model resolution; Sect. 2.3.2). We applied the same basic scheme for soil layer partitioning from LPJmL4.0 (Schaphoff et al., 2018), but continue this scheme down to 20 m (Table A1). We chose a maximum of 20 m soil depth to considerably increase the maximum soil depth compared to constant 3 m in LPJmL4.0, while keeping the increment of computational intensiveness connected to adding more soil layers within an acceptable range. Equal to LPJmL4.0 (Schaphoff et al., 2018), we use a grid cell specific soil texture information which is applied to the whole soil column.

2.2.2 Water balance, infiltration and percolation

We here provide a very brief description of LPJmL's water balance and soil hydrology. A detailed description can be found in Schaphoff et al. (2018).

Hydraulic conductivity and water holding capacity (water content at permanent wilting point, at field capacity, and at saturation) for each grid cell are derived from information on soil texture from the Harmonized World Soil Database (HWSD) version 1 (Nachtergaele et al., 2009) and relationships between texture and hydraulic properties from Cosby et al. (1984). Each soil layer's (Sect. 2.2.1) water content can be altered by infiltrating rainfall and percolation. The soil water content of the first soil layer determines the infiltration rate of rain and irrigation water. The excess water that does not infiltrate generates surface water runoff. Water percolation through the soil layers is calculated by the storage routine technique (Arnold et al., 1990) as used in regional hydrological models such as SWIM (Krysanova et al., 1998). Water percolation thus depends on the hydraulic conductivity of each soil layer and the soil water content between field capacity and saturation at the beginning and the end of the day for all soil layers. Similar to water infiltration into the first soil layer, percolation in each soil layer is limited by the soil moisture of the following lower layer. Excess water over the saturation levels forms lateral runoff in each layer and contributes to subsurface runoff. Surface and subsurface runoff accumulate to river discharge. The routines for water balance, infiltration and percolation were not changed for LPJmL4.0-VR. Thus the routines now apply for soil columns of up to 20 m depth (Sect. 2.2.1).

2.2.3 Diversifying general tree rooting strategies

In LPJmL4.0 the tree rooting strategy of a PFT is reflected by a certain prescribed vertical distribution of fine roots throughout the soil column. Each soil layer l is assigned a PFT specific relative amount of fine roots $rootdist_l$:

$$rootdist_l = rootdist(z_l) - rootdist(z_{l-1}) \qquad \text{Eq. (1)}$$

where z_l is the soil layer boundary depth in cm of each soil layer l and $rootdist(z_l)$ is the relative amount of fine roots between the forest floor and the boundary of soil layer l. The function $rootdist(z)$ is defined following Jackson *et al.* (1996):

$$roodist(z) = \frac{1-\beta^z}{1-\beta^{z_{bottom}}} \qquad \text{Eq. (2)}$$

where β is a constant parameter shaping the vertical distribution of fine roots and therefore determining the tree rooting strategy and z_{bottom} is the maximum soil depth in cm. In LPJmL4.0 each PFT is assigned a different β-value reflecting the average tree rooting strategy on this broad PFT scale (Schaphoff et al., 2018).

To quantify the maximum rooting depth of PFTs that actually results from this approach (Eq. 1&2) we here calculate the depth at which the cumulated fine root biomass from the soil surface downwards is 95% (D_{95_max}) as follows:

$$D_{95\_max} = \frac{log(1-0.95 \cdot (1-\beta^{z_{bottom}}))}{log(\beta)} \qquad \text{Eq. (3)}$$

In LPJmL4.0 the β-values of tropical tree PFTs are set to 0.962 for the tropical broadleaved evergreen tree and to 0.961 for the tropical broadleaved deciduous tree following Jackson et al. (1996). According to Eq. 3 both PFTs have a D_{95_max} smaller than 1 m. For LPJmL4.0-VR we extended this representation of tree rooting strategies by splitting both tropical tree PFTs

168 into 10 sub-PFTs and assigned each with a different β-value. These values were chosen to cover a range of different D_{95_max}

169 values between 0.5 and 18m (Table 1). We chose 18 m as the largest D95_max value in order to avoid that roots of the

170 respective sub-PFT significantly exceed the maximum soil depth of 20 m (see also 2.2.5). Fig. 1 shows the new maximum

171 distribution of fine roots throughout the soil column for the different β-values chosen (Table 1).

2.2.4 Belowground carbon investment

173 Tropical trees can avoid water stress under seasonally dry climate by growing relatively deep roots (Brum et al., 2019; Fan et

174 al., 2017) which goes along with increased below-ground carbon investment. Thus, the need for deep water access creates a

175 trade-off between below-ground and above-ground carbon investment. Therefore, a new carbon allocation scheme for

176 LPJmL4.0-VR was necessary to account for this trade-off in order to reproduce observed local to regional patterns and

177 distributions of tree rooting strategies instead of prescribing them. In LPJmL4.0-VR we introduced two new carbon pools,

178 namely root sapwood and root heartwood. Like stem sapwood in LPJmL4.0, also root sapwood in LPJmL4.0-VR needs to

179 satisfy the assumptions of the pipe model (Shinozaki et al., 1964; Waring et al., 1982). The pipe model describes, that for a

180 certain amount of leaf area a certain amount of water conducting tissue must be available. In LPJmL4.0 the cross-sectional

181 area of stem sapwood needs to be proportional to the leaf area LA_{ind} as follows:

182 $$LA_{ind} = k_{la:sa} \cdot SA_{ind}$$ Eq. (4)

183 where $k_{la:sa}$ is a constant describing the ratio of leaf area and stem sapwood cross-sectional area (SA_{ind}). In LPJmL4.0-VR we

184 also apply the pipe model to root sapwood. Root sapwood cross-sectional area in the first soil layer is equal to stem sapwood

185 cross-sectional area, as all water must be transported through the root sapwood within this soil layer. In the following soil

186 layers downwards, root sapwood cross-sectional area decreases by the relative amount of fine roots in all soil layers above

187 (Fig. 2). Root sapwood is turned into root heartwood at an equal rate as stem sapwood is turned into stem heartwood, i.e. 5%

188 per year as implemented in LPJmL4.0 (see Schaphoff *et al.*, 2018).

2.2.5 Root growth

190 In LPJmL4.0 (Schaphoff et al., 2018) no vertical root growth is simulated, thus the relative distribution of fine roots over the

191 soil column is constant over space and time. It means that PFTs starting from bare ground in a sapling stage display the same

192 relative distribution of fine roots throughout the soil column as a full-grown forest which contradicts the principles of

193 dynamic root growth over a tree's lifetime. Applied to LPJmL4.0-VR, the belowground biomass of an initialized deep

194 rooting-strategy sub-PFT would exceed its aboveground biomass (AGB) by order of magnitudes when acknowledging

195 coarse roots. Consequently, deep rooting strategies would always be disadvantageous, calling for modelling gradual root

196 growth in LPJmL4.0-VR. Unfortunately, little is known about how roots of tropical trees grow over time, given the fact that

197 this research field is strongly time and resource demanding, and at the same time the variety of tree species, rooting

198 strategies and environmental conditions are large (Jenik, 2010). A recent promising study by Brum *et al.* (2019) was able to

199 capture the effective functional rooting depth (EFRD) of different size classes of 12 dominant tree species in a seasonal

200 Amazon forest where tree roots grow considerably deep with maximum values reaching below 30 m. To our knowledge this

201 is the only study capturing the relation between the size of tropical trees and their maximum rooting depth in a high spatial

202 resolution covering sufficient tree-height classes in order to derive a functional relation between tree height and rooting

203 depth. Following the findings of Brum *et al.* (2019), we here implemented a logistic root growth function, which calculates a

204 general maximum conceivable tree rooting depth D depending on tree height:

205 $$D = \frac{S}{e^{-kSh}} \cdot \left(\frac{S}{D_0} - 1\right)$$ Eq. (5)

206 where S is the maximum soil depth in the model (20 m), k is the growth rate (set to 0.02), h is the average tree height of a

207 PFT in m and D_0 is the initial rooting depth of tree PFT saplings (set to 0.1 m; tree saplings in LPJmL4.0-VR are initialized

208 with a height of 0.45 m as in LPJmL4.0). The distribution of fine root biomass of each sub-PFT in the soil column is then

adjusted according to D at each time step, by restricting z_{bottom} in Eq. 2. Every time D crosses a specific soil layer boundary (Sect. 2.2.1) z_{bottom} is assigned the value of the next soil layer boundary. Thus, z_{bottom} increases in discrete steps. Consequently, each tree rooting strategy allowed for in this study (Sect. 2.2.3) shows a logistic growth of rooting depth which is dependent on the sub-PFT height and which saturates towards its specific maximum rooting depth (Fig. 3). Therefore, limitations of aboveground sub-PFT growth due to below-ground carbon investment of different tree rooting strategies (Sect. 2.2.4) are equal in the sapling phase of all sub-PFTs (starting from bare ground) and start to diverge with increasing sub-PFT height. In the case D exceeds the grid cell specific local soil depth (as prescribed by the soil thickness input, see Sect. 2.3.2) all the respective fine root biomass exceeding this soil depth is transferred to the last soil layer matching this soil depth (see also Fig. 2 right panel and Supplementary Video 1 for a visualization of root growth under http://www.pik-potsdam.de/~borissa/LPJmL4_VR/Supplementary_Video_1.pptx).

The parameter k in Eq. 5 was chosen to preserve the slope of the 75%ile function describing the relation between tree height and EFRD as found in Brum *et al.* (2019). We could not implement any of the original functions as suggested in Brum *et al.* (2019) since they deliver unrealistic low values of rooting depth (between 0 and 10cm) for trees <= 10 m, which results in a strong competitive disadvantage against herbaceous PFTs in LPJmL4.0-VR. We decided for the slope of the 75%ile function to allow for root growth rates close to the maximum which also allows for the largest D_{95_max} values in this study (Sect. 2.2.3) to be reached. Note that Brum *et al.* (2019) originally propose a relation between tree diameter at breast height (*DBH*) and EFRD. For our purposes we related rooting depth to tree height (h), which is calculated from DBH in in LPJmL4.0 according to Huang et al. (1992):

$$h = k_{allom2} \cdot DBH^{k_{allom3}} \qquad \text{Eq. (6)}$$

where k_{allom2} and k_{allom3} are constants set to 40 and 0.67, respectively (Schaphoff et al., 2018).

2.2.6 Competition of rooting strategies

In each grid-cell all sub-PFTs of the evergreen and deciduous tree PFTs compete for light and water following LPJmL4.0's approach to simulate plant competition. In LPJmL4.0, the number of new PFT saplings per unit area (est_{PFT} in ind m^{-2} a^{-1}) which are established each year is proportional to a maximum establishment rate k_{est} and to the sum of foliage projected cover (FPC; a relative number between 0 and 1) of all tree PFTs present in a grid cell (FPC_{TREE}). It declines in proportion to canopy light attenuation when the sum of woody FPCs exceeds 0.95, thus simulating a decline in establishment success with canopy closure (Prentice et al., 1993):

$$est_{PFT} = k_{est} \cdot (1 - e^{(-5 \cdot (1-FPC_{TREE})}) \cdot \frac{1- FPC_{TREE}}{n_{est_{TREE}}} \qquad \text{Eq. (7)}$$

where $n_{est_{TREE}}$ is the number of established tree individuals (ind m^{-2} a^{-1}). It is important to note that LPJmL4.0 does not simulate individual trees. As a common method of DGVM's, tree saplings enter the average individual of a PFT as described in Schaphoff et al. (2018).

To allow for environmental filtering of tree rooting strategies which are best adapted to local environmental conditions, we changed the standard tree establishment scheme in LPJmL4.0-VR. Now, the establishment rates of sub-PFTs (est_{sub_PFT}) are additionally weighted by the local dominance of each sub-PFT as follows:

$$est_{sub\_PFT} = k_{est} \cdot \left(1 - e^{-5 \cdot (1-FPC_{TREE})}\right) \cdot \frac{1-FPC_{TREE}}{n_{est_{TREE}}} \cdot \frac{FPC_{sub\_PFT}}{FPC_{TREE}} \cdot n_{est_{TREE}} \qquad \text{Eq. (8)}$$

where FPC_{sub_PFT} is the FPC of each sub-PFT. The new term leads to a higher establishment rate for productive sub-PFTs relative to their spatial dominance and vice versa, without changing the overall establishment rate as set by Prentice et al. (1993). This function has the effect that non-viable sub-PFTs are outcompeted over time.

2.2.7 Background mortality

In LPJmL4.0 background mortality is modelled by a fractional reduction of PFT biomass, which depends on growth efficiency (Schaphoff et al., 2018). This annual rate of mortality is limited by a constant maximum mortality rate of 3% of tree individuals per year which is applied to all tree PFTs. In other words the fastest total biomass loss of a tree PFT due to low growth efficiency can happen within about 33 simulation years. In general, this maximum mortality rate can be regarded as a global tuning parameter of biomass accumulation as it caps the maximum biomass loss. Since many mechanisms influencing tree mortality in the real world, e.g. hydraulic failure (Johnson et al., 2018), are not yet implemented in most DGVMs including LPJmL4.0 (Allen et al., 2015), the parameterization of a background tree mortality remains a challenging topic. Under the current model status of LPJmL4.0 maximum mortality rates are a necessary feature, while future model development must overcome the concept of applying a maximum mortality rate by refining and implementing most important mechanisms that influence tree mortality.

In LPJmL4.0-VR tree PFTs can access water in soil depths which were formerly inaccessible. This enhances the general growth efficiencies of tree PFTs and consequently decreases their overall background mortality. Since global biomass pattern simulated with LPJmL4.0 were already in acceptable range, the maximum background mortality in LPJmL4.0-VR was calibrated and is now increased to 7% in order to counter-balance increased survival rates and therefore biomass accumulation.

2.3 Model input data

2.3.1 Climate input data

All versions of LPJmL used in this study (Sect. 2.4) were forced with 4 different climate inputs each delivering the climate variables air temperature, precipitation, long-wave and shortwave downward radiation at daily or monthly resolution:

1) WATCH Forcing Data (WFD) + WATCH Forcing Data methodology applied to ERAInterim data. A combination of the WATCH data set (Weedon et al., 2011) and the WFDEI data set (Weedon et al., 2014) as used in the ISIMIP project (https://www.isimip.org/gettingstarted/input-data-bias-correction/details/5/). This input data set is called WATCH+WFDEI hereafter.

2) Global Soil Wetness Project Phase 3 (GSWP3) (Kim *et al.*, no date; http://hydro.iis.u-tokyo.ac.jp/GSWP3/index.html).

3) NOAH Global Land Assimilation System version 2.0 (GLDAS, Rodell *et al.*, 2004).

4) Climate forcing as in Schaphoff *et al.* (2018) with monthly precipitation provided by the Global Precipitation Climatology Centre (GPCC Full Data Reanalysis version 7.0; (Becker et al., 2013), daily mean temperature from the Climate Research Unit (CRU TS version 3.23, University of East Anglia Climatic Research Unit, 2015; Harris *et al.*, 2014), shortwave downward radiation and net downward radiation reanalysis data from ERA-Interim (Dee et al., 2011), and number of wet days from (New et al., 2000) used to allocate monthly precipitation to individual days.

This input data set is called CRU hereafter.

2.3.2 Soil and sediment thickness

For this study, we regridded a global 1 x 1 km soil and sediment thickness product (Pelletier et al., 2016) to the 0.5° x 0.5° spatial resolution of LPJmL4.0-VR, set the global maximum value to 20 m according to the maximum soil depth chosen for LPJmL4.0-VR (Sect. 2.2.1), and used the resulting map as grid cell specific model input (Fig. A4). Regridding was done using the software R (R Core Team, 2019) with the package "raster" (Hijmans and van Etten, 2016). We used the aggregate function to calculate the average value of all Pelletier et al. (2016) data entries falling into the coarser 0.5° grid of LPJmL.

2.4 Model versions and simulation protocol

In order to investigate the impact of simulating variable rooting strategies and root growth, we employ 3 model versions of LPJmL in this study: 1) LPJmL4.0, 2) LPJmL4.0-VR, and 3) LPJmL4.0-VR-base. LPJmL4.0-VR-base has the same settings as LPJmL4.0-VR except variable rooting strategies, i.e. using the 2 β-values of LPJmL4.0 for the respective 10 sub-PFTs of the tropical broadleaved evergreen PFT ($\beta = 0.962$) and the tropical broadleaved deciduous PFT ($\beta = 0.961$). We regard LPJmL4.0-VR-base as the baseline model of this study, because comparisons to LPJmL4.0-VR enable to investigate differences caused by the presence or absence of variable tree rooting strategies.

Each simulation was initialized with 5000 simulation years of spin up from bare ground without land-use by periodically cycling the first 30 years of the respective climate data set (1901-1930 for WATCH+WFDEI, GSWP3, CRU and 1948-1977 for GLDAS) and using a pre-industrial atmospheric CO_2 level of 278 ppm. The first spin-up ensures that carbon pools and local distributions of PFTs and sub-PFTs are in equilibrium with climate (Schaphoff et al., 2018). In a second spin up phase cycling the same 30 years of climate data, historical land-use and changing levels of atmospheric CO_2 concentration are introduced. The second spin-up starts in the year 1700 and ends with the first year available in each climate data set. Land-use is updated annually as described in Schaphoff et al. (2018). Before the year 1840 a constant pre-industrial atmospheric CO_2 concentration of 278 ppm is prescribed. After this year atmospheric CO_2 increases annually based on data of Tans and Keeling (2015) as described in Schaphoff et al. (2018). After the second spin up, transient simulations start with the first year available in each climate data set and end in 2010. Land-use and atmospheric CO_2 are consistently updated annually continuing to follow the same data sets as used in the second spin-up.

At the beginning of the first spin-up, all sub-PFTs in LPJmL4.0-VR and LPJmL4.0-VR-base have the same chance to establish, i.e. tree rooting strategies are uniformly distributed. During the spin-up simulations local environmental filtering and competition in connection with PFT-dominance dependent establishment rates (Sect. 2.2.6) determine which tree rooting strategies are best adapted and which are outcompeted. Therefore, the transient simulations already start with distinct distributions of tree rooting strategies.

2.5 Model validation

2.5.1 Validation data

Regional biomass pattern

For evaluation of simulated regional pattern of AGB we compare the results of the 3 LPJmL model versions used in this study to two remote sensing based biomass maps (Avitabile et al., 2016; Saatchi et al., 2011) which were regridded to the spatial resolution of the LPJmL models. Data of Avitabile et al. (2016) was regridded using the software R (R Core Team, 2019) with the package raster (Hijmans and van Etten, 2016). We used the aggregate function to calculate the average value of all Avitabile et al. (2016) data entries falling into the coarser 0.5° grid of LPJmL. Regridded data of Saatchi et al. (2011) was taken from Carvalhais et al. (2014).

Local scale evapotranspiration and productivity

To evaluate simulated local ET and net ecosystem exchange (NEE) of the 3 LPJmL versions used in this study, we compare Fluxnet eddy covariance measurements of ET at 7 sites and NEE at 3 sites across the study region (Bonal *et al.*, 2008; Saleska *et al.*, 2013, Table A2) to respective simulated rates of local ET and NEE. We used only 3 sites for NEE comparisons, because only those sites provided continuous data covering more than 2 years. Fluxnet data was downloaded from https://fluxnet.fluxdata.org (under DOI: 10.18140/FLX/1440032 and DOI: 10.18140/FLX/1440165) in October 2017 and from https://daac.ornl.gov/LBA/guides/CD32_Brazil_Flux_Network.html in November 2019.

Continental scale gridded evapotranspiration products and selection of regions

To evaluate the simulated ET over large regions and during a long period (1981-2010), we use three global gridded datasets: Global Land Data Assimilation System Version 2 (Rodell et al., 2004), ERA-Interim/Land (ERAI-L, Balsamo *et al.*, 2015) and Global Land Evaporation Amsterdam Model v3.2 (GLEAM, Miralles *et al.*, 2011; Martens *et al.*, 2017).

GLDAS and ERAI-L are reanalysis products, meaning that they are land surface models forced with meteorological data that has been corrected with observations to give better estimates of land surface variables. The selection of these two products is based on the study of Sörensson and Ruscica (2018), who found that they have a better performance over South America than other reanalysis and satellite-based ET products. GLDAS uses the land surface model Noah (Ek et al., 2003) forced by Princeton meteorological dataset version 2.2 (Sheffield et al., 2006). The soil depth of Noah is 2 m and the model uses four soil layers and vegetation data from University of Maryland (http://glcf.umd.edu/data/landcover/). ERAI-L uses the land surface model HTESSEL (Hydrology-Tiled ECMWF Scheme for Surface Exchanges over Land, Balsamo *et al.*, 2009) forced by ERA-Interim atmospheric data with a GPCP based correction of monthly precipitation. The soil depth of ERAI-L is 2.89 m, the model uses four soil layers and vegetation data from ECOCLIMAP (Masson et al., 2003).

GLEAM uses the Priestley-Taylor equation to estimate the potential ET and a set of algorithms with meteorological and vegetation satellite data as input to calculate the actual ET. The version used here, GLEAMv3.2a (Martens *et al.*, 2017, downloaded from https://www.gleam.eu/#downloads) uses precipitation input from MSWEP v1.0 (Beck et al., 2017), vegetation cover from the MODIS product MOD44B, remotely sensed Vegetation Optical Index from CCI-LPRM (Liu et al., 2013) and assimilates soil moisture from both remote sensing (ESA CCI SM v2.3, Liu *et al.*, 2012) and land-reanalysis (GLDAS Noah, Rodell *et al.*, 2004). The original spatio-temporal resolution of GLDAS and GLEAM is 0.25º x 0.25º while for ERAI-L it is 0.75º x 0.75º. Monthly time series were calculated from daily values for the three datasets. Hereafter, we use the short names GLDAS, ERAI-L and GLEAM for the described reference datasets.

For the temporal analysis of ET we used five climatological regions across the study area: Northern South America (NSA), Equatorial Amazon West (EQ W), Equatorial Amazon East (EQ E), Southern Amazon (SAMz), and South American Monsoon System region (SAMS) (see Fig. 9f). These regions result from a K-means clustering analysis of the annual cycles of the main drivers of ET: precipitation and surface net radiation (for details see Sörensson and Ruscica, 2018). Additionally we divided the large EQ region used by Sörensson and Ruscica (2018) in two smaller (EQ W and EQ E) at 60ºW, since this is the approximate division between regimes that have a maximum climatological water deficit (MCWD; Sect. 2.5.3) of around -200 mm per year (EQ W), and of around -500 mm per year (EQ E).

Spatial distribution of vegetation types

To evaluate the simulated regional distribution of simulated biome types of the 3 LPJmL versions we compare our results to satellite-derived vegetation composition maps from ESA Land cover CCI V2.0.7 (Li et al., 2018) which were reclassified to the PFTs of LPJmL from Forkel *et al.* (2014). In this dataset PFT dominance is indicated by foliage projected cover (FPC) which is also a standard output variable of the 3 LPJmL model versions allowing a direct comparison to model results.

Spatial pattern of rooting depth

We compare regional patterns of mean rooting depth simulated with LPJmL4.0-VR to a maximum depth of root water uptake map (Fan et al., 2017) which was regridded to the 0.5° x 0.5° spatial resolution of LPJmL4.0-VR. This product was inversely modelled by taking the dynamically interacting variables soil water supply and plant water demand into account. In Fan et al. (2017) supply was based on climate, soil properties and topography and demand of plant transpiration deduced from remotely sensed reanalysis of atmospheric water fluxes and leaf area index (LAI) data.

2.5.2 Validation metrics

Except for inventory biomass all statistical evaluations of model results were based on 1) Pearson Correlation and 2) normalized mean squared error (NME; Kelley *et al.*, 2013). NME is calculated as:

$$NME = \frac{\sum_{i=1}^{N} |y_i - x_i|}{\sum_{i=1}^{N} |x_i - \bar{x}|}$$ <div style="text-align: right">Eq. (9)</div>

where y_i is the simulated and x_i the reference value in the grid cell or time step i. $\bar{x}$ is the mean reference value. NME takes the value 0 at perfect agreement, 1 when the model performs as well as the reference mean and values > 2 indicate complete disagreement.

2.5.3 Maximum cumulative water deficit as indicator of seasonal water stress

To analyse and explain geographical pattern of rooting depth, ET and productivity we use the maximum cumulative water deficit (MCWD) as an independent indicator of potential seasonal water demand of vegetation. MCWD is a widely used indicator for seasonal water stress of tropical and sub-tropical forests in South America (Aragão et al., 2007; Lewis et al., 2011; Malhi et al., 2009). MCWD captures the seasonal difference of ET and precipitation in a cumulative way and therefore comprises dry season strength and duration. Here we calculate MCWD on a monthly basis. Therefore, we first calculate the cumulative water deficit CWD_n of each month n as:

$$CWD_n = CWD_{n-1} - PET_n + P_n$$ <div style="text-align: right">Eq. (10)</div>

where PET is the potential monthly ET and P the monthly sum of precipitation. CWD is constrained to values <=0 and is set to 0 at the end of each hydrological year, here the last day of September, as in Lewis *et al.* (2011). We use *P* from climate input used for model forcing (Sect. 2.3.1) and PET as it is simulated by LPJmL4.0 (Schaphoff et al., 2018) which is only dependent on net surface radiation and air temperature, therefore remaining an explanatory variable independent of vegetation dynamics. We chose this PET instead of using the commonly used constant ET of 100 mm/month to calculate CWD (Aragão et al., 2007; Lewis et al., 2011; Malhi et al., 2009), because in this way, the CWD better corresponds to the actual climatological conditions in the different LPJmL model versions used in this study (Sect. 2.4). MCWD is then calculated as:

$$MCWD_y = min\left(CWD_{October,y-1}, \dots, CWD_{September,y}\right)$$ <div style="text-align: right">Eq. (11)</div>

where *y* indicates the calendrical year.

3 Results

3. 1 Local and regional pattern of tree rooting strategies

In LPJmL4.0-VR the contribution of each tree rooting strategy to the overall net primary productivity (NPP) appears highly dependent on local environmental conditions. Comparisons at the local scale show that shallow-rooted (deep-rooted) sub-PFTs contribute more to the overall NPP under generally wetter (drier) and less (more) seasonal climate conditions (Fig. 4). At the Fluxnet site MAN K34, which exhibits a mean annual precipitation (MAP) of 2609 mm and a mean MCWD of -222 mm under CRU climate input (2001-2010), the sub-PFT with a maximum rooting depth (D_{95_max}) of 0.5 m contributes most to overall NPP and the whole distribution of NPP weighted D_{95_max} classes shows a mean of 1.52 m (Fig. 5a). At the Fluxnet site STM K67, which exhibits a lower MAP of 2144 mm and a stronger dry season reflected in a mean MCWD of -465 mm, the NPP weighted distribution of D_{95_max} shows a peak at 10 m and a corresponding mean of 10.26 m (Fig. 4b). Since both sites have a soil depth of 20 m (according to the soil depth input; Sect. 2.3.2, Fig. A1) differences in rooting strategy compositions must emerge from the climatic differences of those sites. It is important to note that D_{95_max} values in Fig. 4 (i.e. the bins on the x-axes) do not necessarily reflect the true achieved rooting depth of each sub-PFT, but their maximum value. For reasons of visual clarity for this figure we kept the bins of the x-axes as chosen in Table 1.

Based on the information of how much NPP each sub-PFT contributes in each grid cell, we derived maps of mean rooting depth over the whole study region for the time span 2001-2010 for each climate input used in this study (Fig. 5). In contrast to Fig. 4 we computed the mean of the actually achieved D_{95} of each sub-PFT (evergreen and deciduous combined) weighted

by the respective relative NPP contribution of each sub-PFT to total forest NPP (we call $\overline{D_{95}}$). Apparently, the regional pattern of $\overline{D_{95}}$ reflects the effects of climate and soil depth. A general East to West gradient of $\overline{D_{95}}$ over the Amazon region follows climatic gradients of precipitation and MCWD (Fig. A2-A3), while soil depth (Fig. A1) constrains $\overline{D_{95}}$ especially in the South-Eastern Amazon. In general, areas with higher mean annual rainfall and weaker dry season show lower $\overline{D_{95}}$ and vice versa. This pattern holds true under all climate inputs, with some minor local differences and is in line with an inversely modelled global gridded product of maximum depth of root water uptake (MDRU in Fan et al. 2017). Nevertheless, we find considerable absolute differences between MDRU and $\overline{D_{95}}$ (Fig. A4), which can easily emerge from different model settings and assumptions, e.g. related to differences in spatial model resolution, simulated water percolation and underlying vegetation features.

Focussing on the climatological clusters (Sect. 2.5.1 and Fig. 9f) under CRU climate input, the western Amazon (EQ W), with a MAP of 2708 mm and mean MCWD of -163 mm, displays an overall mean $\overline{D_{95}}$ of 1.14 m and a maximum of 5.47 m, despite considerably deeper soils present. In this cluster Fan et al. (2017) find a respective mean and maximum MDRU of 1.26 and 17.95 m. In the Northern, Western and Southern Amazon clusters (NSA, EQ E, SAMz) with lower MAP of 2299, 2190 and 2035 mm and considerably lower MCWD of -488, -438 and -497 mm, respectively, mean $\overline{D_{95}}$ increases to 2.32, 3.20 and 2.68 m, respectively (mean MDRU of 1.85, 2.84 and 3.28 m). Here, maximum $\overline{D_{95}}$ values respectively reach 11.97, 11.27 and 9.04 m (maximum MDRU of 14.28, 13.47 m and 16.57 m). In the monsoon dominated region (SAMS) displaying the lowest MAP of 1449 mm and MCWD of -649 mm, mean $\overline{D_{95}}$ decreases to 1.37 m (mean MDRU 2.61 m). The maximum $\overline{D_{95}}$ of this region reaches 11.17 m located at the border to SAMz (maximum MDRU 49.37 m).

The regional simulation of $\overline{D_{95}}$ now allows us to generalize which tree rooting strategies occupy which climate space. Using MCWD and MAP to define a climate space we find a clear adjustment of $\overline{D_{95}}$ (Fig. 6). A core region with deep-rooted forests (mean $\overline{D_{95}} > 4$ m) is found where MCWD ranges between -1300 and -400 and where MAP is at least 1500 mm (see also maps of MCWD and MAP in Fig. A2-3). This core region is surrounded by a small band of medium rooting depth forests (mean $\overline{D_{95}} \sim$ 2-4 m) forming a crescent shape. Rather shallow-rooted forests (mean $\overline{D_{95}} <$ 2 m) are found in increasingly drier climates where MAP is less than 1000 mm and more increasingly seasonal climates where MCWD is below -500 mm. Shallow-rooted forests are also simulated in very wet conditions where MCWD is greater than -300 mm and MAP is 1200 mm or higher.

3.2 Evapotranspiration rates and productivity

3.2.1 Local evapotranspiration

Differences of intra-annual ET rates between the 3 LPJmL model versions are most pronounced at Fluxnet sites with high seasonality of rainfall (Fig. 7b, e, g and Fig. 8b, e, g). Here, variable tree rooting strategies (LPJmL4.0-VR) lead to a major improvement in reproducing measured Fluxnet NEE and ET, also expressed in reduced NME and increased r^2-values (Table A3-A4). Whereas, constant tree rooting strategies (LPJmL4.0-VR-base and LPJmL4.0) simulate decreasing ET and increasing NEE during dry seasons at these sites, which is anticorrelated to Fluxnet measurements, variable tree rooting strategies (LPJmL4.0-VR) follow the intra-annual Fluxnet signals. Most pronounced improvements are found at STM K67 and STM K83, where the NME of ET and NEE drop below or close to 1, and where r²-values considerably increase compared to the other 2 model versions (Table A3-A4). For STM K67, the r² of NEE is higher under LPJmL4.0 and LPJmL4.0-VR-base, but this refers to a significant anti-correlation.

At STM K77 (Fig. 7f) local circumstances show the influence of variable rooting strategies on ET in a different way. This former rainforest site was converted to pasture before Eddy covariance measurements began. This local land-use at STM K77 is not representative for the respective 0.5° grid cell, and thus all 3 LPJmL model versions simulate mainly natural vegetation instead of pasture. Therefore, the shallow rooting systems of LPJmL4.0 and LPJmL4.0-VR-base show a better

match to ET measurements at STM K77. The site STM K83 (Fig. 7g) is a selectively logged primary forest site which shares the same model grid cell as STM K77 due to their geographical proximity. Again, here only simulations with variable tree rooting strategies (LPJmL4.0-VR) reproduce increased ET and decreased NEE during the dry season. At sites with weaker to no dry season (Fig. 7c, d, h) differences between model versions become less pronounced, as water availability is more stable throughout the year leading to less variable ET.

3.2.2 Continental Evapotranspiration

Results of regional ET are in line with results of site-specific ET. The climatological clusters within the Amazon region which undergo the strongest dry season (EQ E and SAMz) show the largest differences between variable (LPJmL4.0-VR) and constant tree rooting strategies (LPJmL4.0-VR-base and LPJmL4.0). In those clusters LPJmL4.0-VR shows highest agreement with validation data (Fig. 9c, d and Table A5). Agreement is largest for EQ E where NME and r² show values of 0.62 and 0.91, respectively, whereas constant rooting systems in the other 2 model lead to values of NME >= 1.92 and r² <= 0.21 (Table A5). In NSA and EQ W model differences are less pronounced as annual precipitation deficits are lower and deep rooting systems play a lesser role. Still, variable rooting systems lead to noticeably higher agreement in NSA between January and April (Fig. 9a), where monthly precipitation is lower compared to the rest of the year. In the monsoon dominated cluster SAMS outside the Amazon region (Fig. 9e), model differences are least pronounced, since shallow rooting forests dominate this area in LPJmL4.0-VR (Fig. 5) which are very similar to the forests with constant tree rooting strategies in the other 2 model versions.

3.3 Distribution of plant functional types

The simulated relative dominance of tropical tree PFTs across the study area differs substantially between model versions (Fig. 10). In simulations with LPJmL4.0, more than half of the grid cells show the evergreen and deciduous PFTs equally dominant (Fig. 10g-h). Only in areas outside tropical moist climate regions the model tends towards a dominance of the deciduous PFT, whereas e.g. in the Amazon region, the evergreen and deciduous PFTs co-exist in almost equal abundance. These patterns strongly differ from satellite-derived geographical PFT distributions (Fig. 10a-b) and therefore yield in respective comparisons the highest NME values among all models (Table A6). In contrast LPJmL4.0-VR and LPJmL4.0-VR-base show clear dominance patterns of both tropical tree PFTs across the study area (Fig. 10c-f). Nevertheless, differences between LPJmL4.0-VR and LPJmL4.0-VR-base are quite substantial. In LPJmL4.0-VR-base the tropical evergreen PFT dominates the North-Western Amazon region only, negligibly extending further than the borders of climatological clusters NSA and EQ W combined. Beyond these borders the tropical deciduous PFT dominates (Fig. 10e-f). In contrast, in LPJmL4.0-VR (Fig. 10e-f) the evergreen tree PFT dominates the entire Amazon region including EQ E and SAMz, and the deciduous PFT is pushed towards drier and more seasonal climate (including parts of SAMS). Therefore, LPJmL4.0-VR yields lowest NME values in comparison to satellite-derived PFT distributions (Table A6).

3.4 Simulated biomass pattern

3.4.1 Regional pattern of above and belowground biomass

The simulated mean AGB pattern (2001-2010) of LPJmL4.0-VR (Fig. 11c) shows that variable tree rooting strategies lead to a contiguous high biomass over the Amazon region. Especially towards the borders of the South-Eastern Amazon region in the climatological clusters EQ E and SAMz, AGB values appear rather homogenous in contrast to constant shallow tree rooting strategies simulated in the other 2 model versions (Fig. 11d-e). In connection with the significantly improved underlying vegetation composition (Fig. 10e-f) it is clear that LPJmL4.0-VR is the only model version capable of simulating high AGB evergreen rainforests across the climatic gradient of the Amazon region (Fig. A2-A3). This pattern is also found by one satellite derived AGB product chosen for evaluation of our model results (Saatchi *et al.*, 2011; Fig 11b) which yields

a corresponding NME close to 0 (Table A7). However, compared to this product low NME values are found for all model versions. Surprisingly, in comparison to the other AGB validation product (Avitabile et al., 2016a; Fig. 11a) LPJmL4.0-VR-base yields a smaller NME than LPJmL4.0-VR. Considering the significantly less accurate underlying vegetation composition of LPJmL4.0-VR-base as well as LPJmL4.0 (Fig. 10) we regard such comparisons as critical in this context.

Simulating diverse tree rooting strategies in connection with investment into coarse root structures in LPJmL4.0-VR allows analysing carbon investment into the newly implemented root carbon pools (Sect. 2.2.4). As expected, belowground biomass (BGB; Fig. 12) follows the simulated pattern $\overline{D_{95}}$ (Fig. 5). Highest BGB is found at maximum values of $\overline{D_{95}}$ and vice versa.

4 Discussion

4.1 Climate and soil depth determine dominant tree rooting strategies

The geographical patterns of simulated $\overline{D_{95}}$ are very similar under 4 different climate input data sets (Fig. 5). This gives confidence to the general robustness of our results and modelling approach as differences in climate data do not lead to substantially different model behaviour. This is further supported by similar regional rates of ET simulated under the different climate data inputs (Fig. 9).

Simulated $\overline{D_{95}}$ (Fig. 5) clearly follows climate gradients and soil depth found in the study region (Fig. A1-A3). Here, MAP and MCWD can serve as explanatory variables of simulated $\overline{D_{95}}$ (Fig. 6). These findings are in line with the general ecological expectation and former studies that seasonal water depletion of upper soil layers, as a combination of annual precipitation and dry season length and strength, is positively correlated with the rooting depth of tropical evergreen trees (Baker et al., 2009; Ichii et al., 2007; Kleidon and Heimann, 1998, 1999). We also find lower thresholds for MAP and MCWD where $\overline{D_{95}}$ strongly decreases again (Fig. 6) which can be explained by different mechanisms leading to a regime shift from the evergreen to the deciduous tree PFT as discussed below (see 4.2).

To evaluate our model results against empirical data, we checked the data availability on maximum rooting depth across South America in the TRY database (Kattge *et al.*, 2020; data downloaded September 2019). As it is also shown in Fan *et al.* (2017; Fig. 2) we found the number of sites within the TRY data base where maximum rooting depth has been measured in South America to be very low. Moreover, the number of data entries per site appeared very small, where 33 TRY sites falling within our study area showed a mean of ~9 and a median of 6 data entries, while 15 sites showed <=5 data entries. Therefore, we decided to not include site specific comparisons of rooting depth as it is not clear how representative these measurements are for the local forest communities. More research is necessary to increase the number of observation sites and improve the empirical basis of field-based rooting depth to allow for site-specific model evaluation. Nevertheless, as shown in Fan *et al.* (2017; Fig. 2) measured site-specific maximum rooting depth across the Amazon region expectedly follows the known climatic gradient (Fig. A2-A3). The same holds true for the inversely modelled MDRU of Fan *et al.* (2017; we show in Fig. A4), which gives confidence to our results.

4.2 Rooting depth influences the distribution, dominance and biomass of tropical plant functional types

In all 3 model versions used in this study the same land-use is applied (Sect. 2.4), which shapes the geographical extent and maximum dominance of natural vegetation in our results. This is why FPC maps of all model versions show the shape of the Amazon region as a distinct pattern (Fig 10), even though it is less visible for LPJmL4.0-VR-base and one has to consider both tropical tree PFTs at the same time (Fig. 10e-f). Within the Amazon region, LPJmL4.0 simulates a similar dominance of the evergreen and deciduous PFT (Fig. 10g-h), which contradicts evaluation data (Fig. 10a-b) and indicates a similar performance of the 2 PFTs or missing mechanisms rewarding a better performance over time. We here find that introducing a performance dependent tree establishment rate (Sect. 2.2.6) clearly resolves this issue. This feature produces clear dominance pattern of either PFT in LPJmL4.0-VR and LPJmL4.0-VR-base. Apparently, by rewarding better performance,

variable tree rooting strategies (LPJmL4.0-VR) become necessary to reproduce the dominance of the evergreen PFT throughout the Amazon region (Fig. 10e-f). To remain superior in drier and more seasonal environments in the South to South-Eastern Amazon region the evergreen PFT needs to access deep water by adjusting its rooting depth (Fig. 5, 6). Clearly, this adjustment of rooting depth is only possible within a certain climatic frame. Below certain thresholds of MAP (around 1000 mm) and MCWD (around -500 mm) mean $\overline{D_{95}}$ decreases again (Fig. 6), which goes in parallel with a transition from the evergreen to the deciduous PFT. Those thresholds are similar to thresholds between evergreen forests and savanna found by e.g. Malhi *et al.* (2009) at an annual precipitation of 1500 mm and at an MCWD of -300 mm. The substantially lower MCWD value found in this study can be explained by the differences in calculating CWD. While Malhi *et al.* (2009) assume a constant rate of ET per month of 100 mm, we use the monthly variable PET (Sect. 2.5.3). Since PET often is significantly higher than 100 mm our monthly CWD and therefore MCWD values are respectively lower.

Similarly to Malhi *et al.* (2009), Staver, Archibald and Levin (2011) find that the climatic thresholds for evergreen forest are not very distinct and savanna can simultaneously be found in a climatic range around the mean threshold. The authors ascribe this forest-savanna bi-stability to climate-fire-vegetation feedbacks. Many recent studies investigating potential forest-savanna bi-stability and tipping points of forests in and around the Amazon region rely solely on such climatic ranges of tropical biomes (Hirota *et al.*, 2011; Wuyts, Champneys and House, 2017; Zemp *et al.*, 2017; Staal *et al.*, 2018; Ciemer *et al.*, 2019). The results of LPJmL4.0-VR show that knowledge on local tree root adaptations is another important explanatory variable of vegetation cover reducing the uncertainty and width of anticipated climatic ranges where vegetation cover could be bi-stable. These findings are supported by a recent study that finds rooting depth more crucial than fire dynamics for explaining PFT dominance in South America (Langan et al., 2017).

Whether the transition between the evergreen and deciduous tree PFT for the thresholds of MAP and MCWD we find with LPJmL4.0-VR is mainly caused by (a) environmental filtering (including vegetation-fire feedbacks) of deep tree rooting strategies, (b) their competitive exclusion by shallow rooted deciduous sub-PFTs together with the tropical herbaceous PFT (Fig. A6), or most probably a combination of both is yet to be determined. Given that we used the most simplistic fire module of LPJmL (GlobFirm; Thonicke et al., 2001) and current land-use input to allow model evaluation against remotely sensed data in this study, investigating the natural mechanisms of tropical PFT shifts should be in the focus of further studies.

Regardless of the mechanisms that eventually lead to a PFT shift, we can state that neither costs for deep root investment nor a heterogeneous pattern of soil depth across the study region disproves that locally adapted tree rooting depth is key to explain the current geographical distribution of tropical evergreen forests in South-America. Given the large differences between LPJmL4.0-VR and LPJmL4.0-VR-base (Fig. 10) it is clear that in roughly half of the Amazon region the carbon balance of the evergreen PFT is superior to the deciduous PFT only when investing substantial amounts of carbon into deeper roots (Fig. 12). On the one hand this investment has a direct negative effect on productivity, because during growth the allocation of assimilated carbon shifts towards respiring BGB, while investments into productive AGB need to be reduced. On the other hand drier and more seasonal environments show less cloud cover during the dry season (Nemani et al., 2003), enhancing photosynthesis in this time of the year which increases productivity as long as water access is assured (Costa et al., 2010; Wu et al., 2016). The trade-off between AGB and BGB investment most probably leads to a more homogenous AGB pattern across the Amazon region with similar values over a wide climatic range (compare EQ E and SAMz in Fig. 11c-e).

It is important to note that LPJmL4.0-VR appears to underestimate BGB compared to empirical findings in the Amazon region. While LPJmL4.0-VR shows BGB making up a range of 3.6-16.2% of total biomass across the Amazon region, different site specific empirical studies found mean values at the upper end or significantly exceeding this range (Fearnside, 2016). The most plausible explanation for underestimating BGB is that LPJmL4.0-VR does not account for root structures needed for tree statics. Acknowledging tree statics would increase below ground carbon investment and therefore BGB.

569 Nevertheless, below-ground carbon investment for tree statics would apply for all sub-PFTs simultaneously and would
570 therefore most likely not significantly change competition dynamics and resulting distributions of tree rooting strategies
571 found in this study.

572 Comparisons of AGB pattern between all model versions of this study and different biomass products are difficult, since
573 only LPJmL4.0-VR shows a reasonable geographical distribution of underlying PFTs across the study area (Fig. 10, Table
574 A6). Therefore, differences in biomass are not solely the consequence of different productivities directly related to diversity
575 in tree rooting strategies, but also the consequence of simulated PFT dominance, i.e. rather an indirect effect of diversity in
576 tree rooting strategies. Concentrating on LPJmL4.0-VR only, the model matches substantially better with the gridded
577 biomass product of Saatchi et al. (2011; Table A7), since this product shows generally higher biomass values across the
578 Amazon region which are more similar to LPJmL4.0-VR. Therefore, the higher NME found in the comparison to the
579 biomass product of Avitabile et al. (2016) is mainly caused by divergence of mean biomass values of the evergreen PFT
580 across the whole study area rather than pattern divergence. Thus, we argue lowering overall biomass values in LPJmL4.0-
581 VR would improve its match with Avitabile et al. (2016) which is a matter of adjusting overall maximum tree mortality rates
582 (Sect. 2.2.7).

4.3 Diverse tree rooting strategies improve simulated evapotranspiration and productivity

584 LPJmL4.0-VR simulates rates of local ET and NEE which reasonably match respective measurements at different Fluxnet
585 sites throughout the Amazon region (Fig. 7-8), even though we run the model with regionally gridded instead of locally
586 measured climate data. While potentially lacking information on local short-term weather events, gridded climate input still
587 seems to be sufficient to capture broad seasonal signals for our comparisons on a monthly basis. This increases the
588 confidence in our results also on a regional scale.

589 Across large parts of the Amazon region variable tree rooting strategies decrease the intra-annual variability of ET and
590 maintain high rates of NEE and ET during the dry season in accordance with the intra-annual trends suggested by evaluation
591 data (Fig. 7-9). More than that simulated rates of ET and productivity can peak during the dry season e.g. in EQ E which has
592 been explained by increased solar radiation during this time of the year (Nemani et al., 2003; da Rocha et al., 2004).
593 Especially, in EQ E and SAMz at least parts of the forest area must have access to sufficient water in the model and in reality
594 (Costa et al., 2010; Wu et al., 2016). Given that LPJmL4.0-VR and LPJmL4.0-VR-base are essentially identical models with
595 the same soil depth input and subsequent hydrology over the whole soil column, their differences in simulated ET and NEE
596 must emerge from their only difference which is the amount of simulated tree rooting strategies. Therefore, local root
597 adaptations in LPJm4.0-VR can be regarded as a buffer against seasonal precipitation deficits by usage of deep water
598 (exemplary shown for STM K67 in Fig. A7).

599 We can here quantify this water access for the first time on the basis of carbon investment and return, and limited by spatial
600 heterogeneous soil depth. If soil depth was no limit to rooting depth throughout the study region, ET rates of seasonally dry
601 climatological clusters would have most likely been overestimated. The same holds true if deeper roots would not require
602 additional below-ground carbon investment. Therefore, we argue that both factors are of great importance to explain regional
603 rates of ET. This also means that forests in the same climatological cluster contribute very differently to the overall ET and
604 therefore to the moisture transport across South America. We can here mechanistically explain this coherence as we show for
605 the first time on the regional scale how PFTs with variable tree rooting strategies adjust to local environmental conditions
606 and in return lead to simulated rates of ET very close to validation data (Fig. 7, 9). The heterogeneous picture of $\overline{D_{95}}$ we find
607 (Fig. 5) might provide a direct guideline where to put emphasis on forest conservation to maintain continental scale moisture
608 recycling, as $\overline{D_{95}}$ directly scales with rates of ET.

609 Being able to mechanistically reproduce and explain the broad-scale stabilization of water fluxes into the atmosphere has
610 wide implications for DGVM modelling frameworks and simulation of ET as moisture input to the atmosphere in Earth

System Models (ESMs). Our approach can help to better quantify the role of forests for local-to-continental scale moisture recycling and to project the fate of forests under future climate and land-use change. The approach presented here is easily applicable for a wide range of DGVMs and ESMs which simulate fine root distribution in a similar way as the LPJmL model family (based on Jackson *et al.*, 1996). A first and easy to implement step for other models could be to prescribe the relative fine root distribution in a spatial explicit way in accordance to $\overline{D_{95}}$ presented in this study.

5 Conclusions

We here show for the first time that mean tree rooting depth across South-America can indeed explain the spatial distribution of tropical evergreen forests and their spatio-temporal pattern of ecosystem fluxes (ET and NEE) even when the competition of tree rooting strategies, carbon investment into gradually growing roots, and a spatially explicit soil depth are considered. In fact our findings suggest that roughly half of the evergreen forests in the Amazon region depend on investments into rooting systems which go deeper than the standard average PFT parameterization based on literature allows for.

A major advance of the new sub-model version LPJmL4.0-VR is that simulations start with uniform input distributions of tree rooting strategies in each location which shape into a distribution of abundance driven by local environmental filtering and competition. Therefore, these distributions are not a pre-selected input, but an emergent simulation output.

The new model features enable to introduce local tree rooting depth as a key explanatory variable in future studies dealing with potential forest cover bi-stability in tropical regions. Generally, we are convinced that our approach is of high importance to all modelling frameworks of DGVMs and Earth System Models (ESMs) aiming at quantifying continental scale moisture recycling, forest tipping points and resilience. So far the importance of local scale tree root adaptations for regional scale ecosystem functions shows that this potential treasure of below-ground functional diversity must be protected not only in the scope of future global change.

6 Code availability

In case of manuscript acceptance all model code and post-processing scripts will be made available. The first author of this manuscript is also willing to share all information with all reviewers upon request.

7 Data availability

In case of manuscript acceptance all simulation data will be made available. The first author of this manuscript is also willing to share all information with all reviewers upon request.

8 Author contribution

All authors helped in conceptualizing the model. BS and WvB developed the model code. BS, WvB, MD, AS, RR, FL, MB, SB, MH, RO, KT conceived the simulation experiments and BS carried them out. BS, MD, AS, RR and JH analysed model output data. BS prepared the manuscript with contributions from all co-authors.

9 Competing interests

The authors declare that they have no conflict of interest.

11 References

Allen, C. D., Breshears, D. D. and McDowell, N. G.: On underestimation of global vulnerability to tree mortality and forest die-off from hotter drought in the Anthropocene, Ecosphere, 6(8), 1–55, doi:10.1890/ES15-00203.1, 2015.

Aragão, L. E. O. C., Malhi, Y., Roman-Cuesta, R. M., Saatchi, S., Anderson, L. O. and Shimabukuro, Y. E.: Spatial patterns and fire response of recent Amazonian droughts, Geophys. Res. Lett., 34(7), 1–5, doi:10.1029/2006GL028946, 2007.

Arnold, J. G., Williams, J. R., Nicks, A. D. and Sammons, N. B.: SWRRB; a basin scale simulation model for soil and water resources management., SWRRB; a basin scale Simul. Model soil water Resour. Manag., 1990.

Arora, V. K. and Boer, G. J.: A Representation of Variable Root Distribution in Dynamic Vegetation Models, Earth Interact., 7(6), 1–19, doi:10.1175/1087-3562(2003)007<0001:arovrd>2.0.co;2, 2003.

Avitabile, V., Herold, M., Heuvelink, G. B. M., Lewis, S. L., Phillips, O. L., Asner, G. P., Armston, J., Ashton, P. S., Banin, L., Bayol, N., Berry, N. J., Boeckx, P., de Jong, B. H. J., Devries, B., Girardin, C. A. J., Kearsley, E., Lindsell, J. A., Lopez-Gonzalez, G., Lucas, R., Malhi, Y., Morel, A., Mitchard, E. T. A., Nagy, L., Qie, L., Quinones, M. J., Ryan, C. M., Ferry, S. J. W., Sunderland, T., Laurin, G. V., Gatti, R. C., Valentini, R., Verbeeck, H., Wijaya, A. and Willcock, S.: An integrated pan-tropical biomass map using multiple reference datasets, Glob. Chang. Biol., 22(4), 1406–1420, doi:10.1111/gcb.13139, 2016.

Baker, I. T., Prihodko, L., Denning, A. S., Goulden, M., Miller, S. and Da Rocha, H. R.: Seasonal drought stress in the amazon: Reconciling models and observations, J. Geophys. Res. Biogeosciences, 114(1), 1–10, doi:10.1029/2007JG000644, 2008.

Baker, I. T., Prihodko, L., Denning, A. S., Goulden, M., Miller, S. and Da Rocha, H. R.: Seasonal drought stress in the amazon: Reconciling models and observations, J. Geophys. Res. Biogeosciences, 114(1), 1–10, doi:10.1029/2007JG000644, 2009.

Balsamo, G., Viterbo, P., Beijaars, A., van den Hurk, B., Hirschi, M., Betts, A. K. and Scipal, K.: A revised hydrology for the ECMWF model: Verification from field site to terrestrial water storage and impact in the integrated forecast system, J. Hydrometeorol., 10(3), 623–643, doi:10.1175/2008JHM1068.1, 2009.

Balsamo, G., Albergel, C., Beljaars, A., Boussetta, S., Brun, E., Cloke, H., Dee, D., Dutra, E., Munõz-Sabater, J., Pappenberger, F., De Rosnay, P., Stockdale, T. and Vitart, F.: ERA-Interim/Land: A global land surface reanalysis data set, Hydrol. Earth Syst. Sci., 19(1), 389–407, doi:10.5194/hess-19-389-2015, 2015.

Baudena, M., Dekker, S. C., van Bodegom, P. M., Cuesta, B., Higgins, S. I., Lehsten, V., Reick, C. H., Rietkerk, M., Scheiter, S., Yin, Z., Zavala, M. A. and Brovkin, V.: Forests, savannas and grasslands: bridging the knowledge gap between

ecology and Dynamic Global Vegetation Models, Biogeosciences Discuss., 11(6), 9471–9510, doi:10.5194/bgd-11-9471-2014, 2014.

Beck, H. E., Van Dijk, A. I. J. M., Levizzani, V., Schellekens, J., Miralles, D. G., Martens, B. and De Roo, A.: MSWEP: 3-hourly 0.25° global gridded precipitation (1979-2015) by merging gauge, satellite, and reanalysis data, Hydrol. Earth Syst. Sci., 21(1), 589–615, doi:10.5194/hess-21-589-2017, 2017.

Becker, A., Finger, P., Meyer-Christoffer, A., Rudolf, B., Schamm, K., Schneider, U. and Ziese, M.: A description of the global land-surface precipitation data products of the Global Precipitation Climatology Centre with sample applications including centennial (trend) analysis from 1901-present, Earth Syst. Sci. Data, 5(1), 71–99, doi:10.5194/essd-5-71-2013, 2013.

Best, M. J., Pryor, M., Clark, D. B., Rooney, G. G., Essery, R. . L. H., Ménard, C. B., Edwards, J. M., Hendry, M. A., Porson, A., Gedney, N., Mercado, L. M., Sitch, S., Blyth, E., Boucher, O., Cox, P. M., Grimmond, C. S. B. and Harding, R. J.: The Joint UK Land Environment Simulator (JULES), model description – Part 1: Energy and water fluxes, Geosci. Model Dev., 4(3), 677–699, doi:10.5194/gmd-4-677-2011, 2011.

Bonal, D., Bosc, A., Ponton, S., Goret, J., Burban, B., Gross, P., Bonnefonds, J. M., Elbers, J. A., Longdoz, B., Epron, D., Guehl, J. and Granier, A.: Impact of severe dry season on net ecosystem exchange in the Neotropical rainforest of French Guiana, , 14(8), 1917–1933 [online] Available from: https://edepot.wur.nl/1900, 2008.

Brum, M., Vadeboncoeur, M. A., Ivanov, V., Asbjornsen, H., Saleska, S., Alves, L. F., Penha, D., Dias, J. D., Aragão, L. E. O. C., Barros, F., Bittencourt, P., Pereira, L. and Oliveira, R. S.: Hydrological niche segregation defines forest structure and drought tolerance strategies in a seasonal Amazon forest, J. Ecol., 107(1), 318–333, doi:10.1111/1365-2745.13022, 2019.

Brunner, I., Herzog, C., Dawes, M. A., Arend, M. and Sperisen, C.: How tree roots respond to drought, Front. Plant Sci., 6(JULY), 1–16, doi:10.3389/fpls.2015.00547, 2015.

Canadell, J., Jackson, R. B., Ehleringer, J. R., Mooney, H. A., Sala, O. E. and Schulze, E.-D.: Max rooting depth of vegetation types at the global scale, Oecologica, 108, 583–595, doi:10.1007/s10705-016-9812-z, 1996.

Carvalhais, N., Forkel, M., Khomik, M., Bellarby, J., Jung, M., Migliavacca, M., Saatchi, S., Santoro, M., Thurner, M. and Weber, U.: Global covariation of carbon turnover times with climate in terrestrial ecosystems, Nature, 514(7521), 213–217, 2014.

Ciemer, C., Boers, N., Hirota, M., Kurths, J., Müller-Hansen, F., Oliveira, R. S. and Winkelmann, R.: Higher resilience to climatic disturbances in tropical vegetation exposed to more variable rainfall, Nat. Geosci., 12(March), doi:10.1038/s41561-019-0312-z, 2019.

Cosby, B. J., Hornberger, G. M., Clapp, R. B. and Ginn, T.: A statistical exploration of the relationships of soil moisture characteristics to the physical properties of soils, Water Resour. Res., 20(6), 682–690, 1984.

Costa, M. H., Biajoli, M. C., Sanches, L., Malhado, A. C. M., Hutyra, L. R., Da Rocha, H. R., Aguiar, R. G. and De Araújo, A. C.: Atmospheric versus vegetation controls of Amazonian tropical rain forest evapotranspiration: Are the wet and seasonally dry rain forests any different?, J. Geophys. Res. Biogeosciences, 115(4), 1–9, doi:10.1029/2009JG001179, 2010.

Dee, D. P., Uppala, S. M., Simmons, A. J., Berrisford, P., Poli, P., Kobayashi, S., Andrae, U., Balmaseda, M. A., Balsamo, G., Bauer, P., Bechtold, P., Beljaars, A. C. M., van de Berg, L., Bidlot, J., Bormann, N., Delsol, C., Dragani, R., Fuentes, M., Geer, A. J., Haimberger, L., Healy, S. B., Hersbach, H., Hólm, E. V., Isaksen, L., Kållberg, P., Köhler, M., Matricardi, M., Mcnally, A. P., Monge-Sanz, B. M., Morcrette, J. J., Park, B. K., Peubey, C., de Rosnay, P., Tavolato, C., Thépaut, J. N. and Vitart, F.: The ERA-Interim reanalysis: Configuration and performance of the data assimilation system, Q. J. R. Meteorol. Soc., 137(656), 553–597, doi:10.1002/qj.828, 2011.

Ek, M. B., Mitchell, K. E., Lin, Y., Rogers, E., Grunmann, P., Koren, V., Gayno, G. and Tarpley, J. D.: Implementation of Noah land surface model advances in the National Centers for Environmental Prediction operational mesoscale Eta model, J. Geophys. Res. D Atmos., 108(22), 1–16, doi:10.1029/2002jd003296, 2003.

Eshel, A. and Grünzweig, J. M.: Root-shoot allometry of tropical forest trees determined in a large-scale aeroponic system, Ann. Bot., 112(2), 291–296, doi:10.1093/aob/mcs275, 2013.

Fan, Y., Miguez-Macho, G., Jobbágy, E. G., Jackson, R. B. and Otero-Casal, C.: Hydrologic regulation of plant rooting depth., Proc. Natl. Acad. Sci. U. S. A., 114(40), 10572–10577, doi:10.1073/pnas.1712381114, 2017.

Fearnside, P. M.: Brazil's Amazonian forest carbon: the key to Southern Amazonia's significance for global climate, Reg. Environ. Chang., 18(1), 47–61, doi:10.1007/s10113-016-1007-2, 2016.

Forkel, M., Carvalhais, N., Schaphoff, S., Bloh, W. V., Migliavacca, M., Thurner, M. and Thonicke, K.: Identifying environmental controls on vegetation greenness phenology through model-data integration, Biogeosciences, 11(23), 7025–7050, doi:10.5194/bg-11-7025-2014, 2014.

Guimberteau, M., Zhu, D., Maignan, F., Huang, Y., Yue, C., Dantec-Nédélec, S., Ottlé, C., Jornet-Puig, A., Bastos, A., Laurent, P., Goll, D., Bowring, S., Chang, J., Guenet, B., Tifafi, M., Peng, S., Krinner, G., Ducharne, A., Wang, F., Wang, T., Wang, X., Wang, Y., Yin, Z., Lauerwald, R., Joetzjer, E., Qiu, C., Kim, H. and Ciais, P.: ORCHIDEE-MICT (revision 4126), a land surface model for the high-latitudes: model description and validation, Geosci. Model Dev. Discuss., (June), 1–65, doi:10.5194/gmd-2017-122, 2017.

Harris, I., Jones, P. D., Osborn, T. J. and Lister, D. H.: Updated high-resolution grids of monthly climatic observations - the CRU TS3.10 Dataset, Int. J. Climatol., 34(3), 623–642, doi:10.1002/joc.3711, 2014.

Hijmans, R. J. and van Etten, J.: raster: Geographic data analysis and modeling, R Packag. version, 2(8), 2016.

Hirota, M., Holmgren, M., Van New, E. H. and Scheffer, M.: Global Resilience of Tropical Forest, Science (80-.)., 334(October), 232–235, doi:10.1126/science.1210657, 2011.

Huang, S., Titus, S. J. and Wiens, D. P.: Comparison of nonlinear height–diameter functions for major Alberta tree species, Can. J. For. Res., 22(9), 1297–1304, 1992.

Huntingford, C., Zelazowski, P., Galbraith, D., Mercado, L. M., Sitch, S., Fisher, R., Lomas, M., Walker, A. P., Jones, C. D., Booth, B. B. B., Malhi, Y., Hemming, D., Kay, G., Good, P., Lewis, S. L., Phillips, O. L., Atkin, O. K., Lloyd, J., Gloor, E., Zaragoza-Castells, J., Meir, P., Betts, R., Harris, P. P., Nobre, C., Marengo, J. and Cox, P. M.: Simulated resilience of tropical rainforests to CO 2 -induced climate change, Nat. Geosci., 6(4), 268–273, doi:10.1038/ngeo1741, 2013.

Ichii, K., Hashimoto, H., White, M. A., Potter, C., Hutyra, L. R., Huete, A. R., Myneni, R. B. and Nemani, R. R.: Constraining rooting depths in tropical rainforests using satellite data and ecosystem modeling for accurate simulation of gross primary production seasonality, Glob. Chang. Biol., 13(1), 67–77, doi:10.1111/j.1365-2486.2006.01277.x, 2007.

Jackson, R. B., Canadell, J., Ehleringer, J., Mooney, H., Sala, O. and Schulze, E.: A global analysis of root distributions for terrestrial biomes, Oecologica, 108, 389–411, 1996.

Jenik, J.: Roots and root systems in tropical trees, Trop. trees as living Syst., 323, 2010.

Jobbágy, E. G. and Jackson, R. B.: the Vertical Distribution of Soil Organic Carbon and Its Relation To Climate and Vegetation, Ecol. Appl., 10(2), 423–436, doi:10.1890/1051-0761(2000)010[0423:TVDOSO]2.0.CO;2, 2000.

Johnson, D. M., Domec, J. C., Carter Berry, Z., Schwantes, A. M., McCulloh, K. A., Woodruff, D. R., Wayne Polley, H., Wortemann, R., Swenson, J. J., Scott Mackay, D., McDowell, N. G. and Jackson, R. B.: Co-occurring woody species have diverse hydraulic strategies and mortality rates during an extreme drought, Plant Cell Environ., 41(3), 576–588, doi:10.1111/pce.13121, 2018.

Kattge, J., Bönisch, G., Díaz, S., Lavorel, S., Prentice, I. C., Leadley, P., Tautenhahn, S., Werner, G. D. A., Aakala, T. and Abedi, M.: TRY plant trait database–enhanced coverage and open access, Glob. Chang. Biol., 2020.

Kelley, D. I., Prentice, I. C., Harrison, S. P., Wang, H., Simard, M., Fisher, J. B. and Willis, K. O.: A comprehensive benchmarking system for evaluating global vegetation models, Biogeosciences, 10(5), 3313–3340, doi:10.5194/bg-10-3313-2013, 2013.

Kim, H., Watanabe, E.-C., Chang, K., Yoshimura, Y., Hirabayashi, J., Famiglietti, T. and Oki, T.: Century long observation

constrained global dynamic downscaling and hydrologic implication, n.d.

Kim, Y., Knox, R. G., Longo, M., Medvigy, D., Hutyra, L. R., Pyle, E. H., Wofsy, S. C., Bras, R. L. and Moorcroft, P. R.: Seasonal carbon dynamics and water fluxes in an Amazon rainforest, Glob. Chang. Biol., 18(4), 1322–1334, doi:10.1111/j.1365-2486.2011.02629.x, 2012.

Kleidon, A. and Heimann, M.: A method of determining rooting depth from a terrestrial biosphere model and its impacts on the global water and carbon cycle, Glob. Chang. Biol., 4(3), 275–286, doi:10.1046/j.1365-2486.1998.00152.x, 1998.

Kleidon, A. and Heimann, M.: Deep-rooted vegetation, Amazonian deforestation, and climate: Results from a modelling study, Glob. Ecol. Biogeogr., 8(5), 397–405, doi:10.1046/j.1365-2699.1999.00150.x, 1999.

Kleidon, A. and Heimann, M.: Assessing the role of deep rooted vegetation in the climate system with model simulations: Mechanism, comparison to observations and implications for Amazonian deforestation, Clim. Dyn., 16(2–3), 183–199, doi:10.1007/s003820050012, 2000.

Krysanova, V., Müller-Wohlfeil, D.-I. and Becker, A.: Development and test of a spatially distributed hydrological/water quality model for mesoscale watersheds, Ecol. Modell., 106(2–3), 261–289, 1998.

Langan, L., Higgins, S. I. and Scheiter, S.: Climate-biomes, pedo-biomes or pyro-biomes: which world view explains the tropical forest–savanna boundary in South America?, J. Biogeogr., 44(10), 2319–2330, doi:10.1111/jbi.13018, 2017.

Lawrence, D. M., Oleson, K. W., Flanner, M. G., Thornton, P. E., Swenson, S. C., Lawrence, P. J., Zeng, X., Yang, Z.-L., Levis, S., Sakaguchi, K., Bonan, G. B. and Slater, A. G.: Parameterization improvements and functional and structural advances in Version 4 of the Community Land Model, J. Adv. Model. Earth Syst., 3(3), 1–27, doi:10.1029/2011ms000045, 2011.

Lee, J. E., Oliveira, R. S., Dawson, T. E. and Fung, I.: Root functioning modifies seasonal climate, Proc. Natl. Acad. Sci. U. S. A., 102(49), 17576–17581, doi:10.1073/pnas.0508785102, 2005.

Leuschner, C., Moser, G., Bertsch, C., Röderstein, M. and Hertel, D.: Large altitudinal increase in tree root/shoot ratio in tropical mountain forests of Ecuador, Basic Appl. Ecol., 8(3), 219–230, 2007.

Lewis, S. L., Brando, P. M., Phillips, O. L., Van Der Heijden, G. M. F. and Nepstad, D.: The 2010 Amazon drought, Science (80-.)., 331(6017), 554, doi:10.1126/science.1200807, 2011.

Li, W., Houghton, R. A., Bontemps, S., MacBean, N., Lamarche, C., Ciais, P., Peng, S. and Defourny, P.: Gross and net land cover changes in the main plant functional types derived from the annual ESA CCI land cover maps (1992–2015), Earth Syst. Sci. Data, 10(1), 219–234, doi:10.5194/essd-10-219-2018, 2018.

Liu, L., Peng, S., AghaKouchak, A., Huang, Y., Li, Y., Qin, D., Xie, A. and Li, S.: Broad Consistency Between Satellite and Vegetation Model Estimates of Net Primary Productivity Across Global and Regional Scales, J. Geophys. Res. Biogeosciences, 123(12), 3603–3616, doi:10.1029/2018JG004760, 2018.

Liu, Y., Piao, S., Lian, X., Ciais, P. and Smith, W. K.: Seasonal responses of terrestrial carbon cycle to climate variations in CMIP5 models: Evaluation and projection, J. Clim., 30(16), 6481–6503, doi:10.1175/JCLI-D-16-0555.1, 2017.

Liu, Y. Y., Dorigo, W. A., Parinussa, R. M., De Jeu, R. A. M., Wagner, W., McCabe, M. F., Evans, J. P. and Van Dijk, A. I. J. M.: Trend-preserving blending of passive and active microwave soil moisture retrievals, Remote Sens. Environ., 123(October 2006), 280–297, doi:10.1016/j.rse.2012.03.014, 2012.

Liu, Y. Y., van Dijk, A. I. J. M., McCabe, M. F., Evans, J. P. and de Jeu, R. A. M.: Global vegetation biomass change (1988-2008) and attribution to environmental and human drivers, Glob. Ecol. Biogeogr., 22(6), 692–705, doi:10.1111/geb.12024, 2013.

Malhi, Y., Aragao, L. E. O. C., Galbraith, D., Huntingford, C., Fisher, R., Zelazowski, P., Sitch, S., McSweeney, C. and Meir, P.: Exploring the likelihood and mechanism of a climate-change-induced dieback of the Amazon rainforest, Proc. Natl. Acad. Sci., 106(49), 20610–20615, doi:10.1073/pnas.0804619106, 2009.

Markewitz, D., Devine, S., Davidson, E. A., Brando, P. and Nepstad, D. C.: Soil moisture depletion under simulated drought

813   in the Amazon: Impacts on deep root uptake, New Phytol., 187(3), 592–607, doi:10.1111/j.1469-8137.2010.03391.x, 2010.

814   Martens, B., Miralles, D. G., Lievens, H., Van Der Schalie, R., De Jeu, R. A. M., Fernández-Prieto, D., Beck, H. E., Dorigo,

815   W. A. and Verhoest, N. E. C.: GLEAM v3: Satellite-based land evaporation and root-zone soil moisture, Geosci. Model

816   Dev., 10(5), 1903–1925, doi:10.5194/gmd-10-1903-2017, 2017.

817   Masson, V., Champeaux, J. L., Chauvin, F., Meriguet, C. and Lacaze, R.: A global database of land surface parameters at 1-

818   km resolution in meteorological and climate models, J. Clim., 16(9), 1261–1282, doi:10.1175/1520-0442-16.9.1261, 2003.

819   Miralles, D. G., Holmes, T. R. H., De Jeu, R. A. M., Gash, J. H., Meesters, A. G. C. A. and Dolman, A. J.: Global land-

820   surface evaporation estimated from satellite-based observations, Hydrol. Earth Syst. Sci., 15(2), 453–469, doi:10.5194/hess-

821   15-453-2011, 2011.

822   Mokany, K., Raison, R. J. and Prokushkin, A. S.: Critical analysis of root: Shoot ratios in terrestrial biomes, Glob. Chang.

823   Biol., 12(1), 84–96, doi:10.1111/j.1365-2486.2005.001043.x, 2006.

824   Nachtergaele, F. van, Velthuizen, H., Verelst, L., Batjes, N., Dijkshoorn, K. van Engelen, V., Fischer, G., Jones, A.,

825   Montanarella, L. and Petri, M.: Harmonized world soil database, Food and Agriculture Organization of the United Nations,

826   [online] Available from: http://www.fao.org/soils-portal/soil-survey/soil-maps-and-databases/harmonized-world-soil-

827   database-v12/en/, 2009.

828   Nemani, R. R., Keeling, C. D., Hashimoto, H., Jolly, W. M., Piper, S. C., Tucker, C. J., Myneni, R. B. and Running, S. W.:

829   Climate-driven increases in global terrestrial net primary production from 1982 to 1999, Science (80-.)., 300(5625), 1560–

830   1563, doi:10.1126/science.1082750, 2003.

831   Nepstad, D. C., de Carvalho, C. R., Davidson, E. A., Jipp, P. H., Lefebvre, P. A., Negreiros, G. H., da Silva, E. D., Stone, T.

832   A., Trumbore, S. E. and Vieira, S.: The role of deep roots in the hydrological and carbon cycles of Amazonian forests and

833   pastures, Nature, 372(6507), 666–669, doi:10.1038/372666a0, 1994.

834   New, M., Hulme, M. and Jones, P.: Representing twentieth century space-time climate variability. Part II: development of a

835   1901-1996 monthly grids of terrestrial surface climate, J. Clim., 13, 2217–2238, 2000.

836   Nikolova, P. S., Zang, C. and Pretzsch, H.: Combining tree-ring analyses on stems and coarse roots to study the growth

837   dynamics of forest trees: A case study on Norway spruce (Picea abies [L.] H. Karst), Trees - Struct. Funct., 25(5), 859–872,

838   doi:10.1007/s00468-011-0561-y, 2011.

839   Ostle, N. J., Smith, P., Fisher, R., Ian Woodward, F., Fisher, J. B., Smith, J. U., Galbraith, D., Levy, P., Meir, P., McNamara,

840   N. P. and Bardgett, R. D.: Integrating plant-soil interactions into global carbon cycle models, J. Ecol., 97(5), 851–863,

841   doi:10.1111/j.1365-2745.2009.01547.x, 2009.

842   Pelletier, J. D., Broxton, P. D., Hazenberg, P., Zeng, X., Troch, P. A., Niu, G.-Y., Williams, Z., Brunke, M. A. and Gochis,

843   D.: A gridded global data set of soil, intact regolith, and sedimentary deposit thicknesses for regional and global land surface

844   modeling, J. Adv. Model. Earth Syst., 8, 41–65, doi:10.1002/2017MS001065, 2016.

845   Poorter, H., Niklas, K. J., Reich, P. B., Oleksyn, J., Poot, P. and Mommer, L.: Biomass allocation to leaves, stems and roots:

846   meta-analyses of interspecific variation and environmental control, New Phytol., 193(1), 30–50, 2012.

847   Prentice, I. C., Sykes, M. T. and Cramer, W.: A simulation model for the transient effects of climate change on forest

848   landscapes, Ecol. Modell., 65(1–2), 51–70, 1993.

849   R Core Team: R: A language and environment for statistical computing. R Foundatoin for Statistical Computing, [online]

850   Available from: https://www.r-project.org/, 2019.

851   Restrepo-Coupe, N., Levine, N. M., Christoffersen, B. O., Albert, L. P., Wu, J., Costa, M. H., Galbraith, D., Imbuzeiro, H.,

852   Martins, G., da Araujo, A. C., Malhi, Y. S., Zeng, X., Moorcroft, P. and Saleska, S. R.: Do dynamic global vegetation

853   models capture the seasonality of carbon fluxes in the Amazon basin? A data-model intercomparison, Glob. Chang. Biol.,

854   23(1), 191–208, doi:10.1111/gcb.13442, 2017.

855   Rodell, M., Houser, P. R., Jambor, U., Gottschalck, J., Mitchell, K., Meng, C.-J., Arsenault, K., Cosgrove, B., Radakovich,

856 J., Bosilovich, M., Entin, J. K., Walker, J. P., Lohmann, D. and Toll, D.: The Global Land Data Assimilation System, Bull.

857 Am. Meteorol. Soc., 85(March), 381–394, 2004.

858 Saatchi, S. S., Harris, N. L., Brown, S., Lefsky, M., Mitchard, E. T. A., Salas, W., Zutta, B. R., Buermann, W., Lewis, S. L.,

859 Hagen, S., Petrova, S., White, L., Silman, M. and Morel, A.: Benchmark map of forest carbon stocks in tropical regions

860 across three continents, Proc. Natl. Acad. Sci., 108(24), 9899–9904, doi:10.1073/pnas.1019576108, 2011.

861 Saleska, S. R., Da Rocha, H. R., Huete, A. R., Nobre, A. D., Artaxo, P. E. and Shimabukuro, Y. E.: LBA-ECO CD-32 Flux

862 Tower Network Data Compilation, Brazilian Amazon: 1999-2006, , doi:10.3334/ORNLDAAC/1174, 2013.

863 Schaphoff, S., von Bloh, W., Rammig, A., Thonicke, K., Biemans, H., Forkel, M., Gerten, D., Heinke, J., Jägermeyr, J.,

864 Knauer, J., Langerwisch, F., Lucht, W., Müller, C., Rolinski, S. and Waha, K.: LPJmL4 – a dynamic global vegetation

865 model with managed land – Part 1: Model description, Geosci. Model Dev., 11(4), 1343–1375, doi:10.5194/gmd-11-1343-

866 2018, 2018.

867 Schymanski, S. J., Sivapalan, M., Roderick, M. L., Beringer, J. and Hutley, L. B.: An optimality-based model of the coupled

868 soil moisture and root dynamics, Hydrol. Earth Syst. Sci., 12(3), 913–932, doi:10.5194/hess-12-913-2008, 2008.

869 Sheffield, J., Goteti, G. and Wood, E. F.: Development of a 50-year high-resolution global dataset of meteorological forcings

870 for land surface modeling, J. Clim., 19(13), 3088–3111, doi:10.1175/JCLI3790.1, 2006.

871 Shinozaki, K., Yoda, K. and Kira, T.: A quantitative analysis of plant form - The pipe model theory, Japanese J. Ecol., 14(3),

872 1964.

873 Smith, B., Wärlind, D., Arneth, A., Hickler, T., Leadley, P., Siltberg, J. and Zaehle, S.: Implications of incorporating N

874 cycling and N limitations on primary production in an individual-based dynamic vegetation model, Biogeosciences, 11(7),

875 2027–2054, doi:10.5194/bg-11-2027-2014, 2014.

876 Sörensson, A. A. and Ruscica, R. C.: Intercomparison and Uncertainty Assessment of Nine Evapotranspiration Estimates

877 Over South America, Water Resour. Res., 54(4), 2891–2908, doi:10.1002/2017WR021682, 2018.

878 Staal, A., Tuinenburg, O. A., Bosmans, J. H. C., Holmgren, M., Van Nes, E. H., Scheffer, M., Zemp, D. C. and Dekker, S.

879 C.: Forest-rainfall cascades buffer against drought across the Amazon, Nat. Clim. Chang., 8(6), 539–543,

880 doi:10.1038/s41558-018-0177-y, 2018.

881 Stahl, C., Hérault, B., Rossi, V., Burban, B., Bréchet, C. and Bonal, D.: Depth of soil water uptake by tropical rainforest

882 trees during dry periods: Does tree dimension matter?, Oecologia, 173(4), 1191–1201, doi:10.1007/s00442-013-2724-6,

883 2013.

884 Staver, A. C., Archibald, S. and Levin, S. A.: The global extent and determinants of savanna and forest as alternative biome

885 states, Science (80-.)., 334(6053), 230–232, doi:10.1126/science.1210465, 2011.

886 Tans, P. and Keeling, R.: Trends in Atmospheric Carbon Dioxide, Natl. Ocean. Atmos. Adm. Earth Syst. Res. Lab. [online]

887 Available from: http://www.esrl.noaa.gov/gmd/ccgg/trends, 2015.

888 Thonicke, K., Venevsky, S., Sitch, S. and Cramer, W.: The role of fire disturbance for global vegetation dynamics: Coupling

889 fire into a dynamic global vegetation model, Glob. Ecol. Biogeogr., 10(6), 661–677, doi:10.1046/j.1466-822X.2001.00175.x,

890 2001.

891 Waring, R. H., Schroeder, P. E. and Oren, R.: Application of the pipe model theory to predict canopy leaf area, Can. J. For.

892 Res., 12(3), 556–560, doi:https://doi.org/10.1139/x82-086, 1982.

893 Warren, J. M., Hanson, P. J., Iversen, C. M., Kumar, J., Walker, A. P. and Wullschleger, S. D.: Root structural and

894 functional dynamics in terrestrial biosphere models - evaluation and recommendations, New Phytol., 205(1), 59–78,

895 doi:10.1111/nph.13034, 2015a.

896 Warren, J. M., Hanson, P. J., Iversen, C. M., Kumar, J., Walker, A. P. and Wullschleger, S. D.: Root structural and

897 functional dynamics in terrestrial biosphere models - evaluation and recommendations, New Phytol., 205(1), 59–78,

898 doi:10.1111/nph.13034, 2015b.

Weber, U., Jung, M., Reichstein, M., Beer, C., Braakhekke, M. C., Lehsten, V., Ghent, D., Kaduk, J., Viovy, N., Ciais, P., Gobron, N. and Rödenbeck, C.: The interannual variability of Africa's ecosystem productivity: A multi-model analysis, Biogeosciences, 6(2), 285–295, doi:10.5194/bg-6-285-2009, 2009.

Weedon, G. P., Gomes, S., Viterbo, P., Shuttleworth, W. J., Blyth, E., Österle, H., Adam, J. C., Bellouin, N., Boucher, O. and Best, M.: Creation of the WATCH Forcing Data and Its Use to Assess Global and Regional Reference Crop Evaporation over Land during the Twentieth Century, J. Hydrometeorol., 12(5), 823–848, doi:10.1175/2011jhm1369.1, 2011.

Weedon, G. P., Balsamo, G., Bellouin, N., Gomes, S., Best, M. J. and Viterbo, P.: Data methodology applied to ERA-Interim reanalysis data, Water Resour. Res., 50, 7505–7514, doi:10.1002/2014WR015638.Received, 2014.

Wu, J., Albert, L. P., Lopes, A. P., Restrepo-Coupe, N., Hayek, M., Wiedemann, K. T., Guan, K., Stark, S. C., Christoffersen, B., Prohaska, N., Tavares, J. V., Marostica, S., Kobayashi, H., Ferreira, M. L., Campos, K. S., Dda Silva, R., Brando, P. M., Dye, D. G., Huxman, T. E., Huete, A. R., Nelson, B. W. and Saleska, S. R.: Leaf development and demography explain photosynthetic seasonality in Amazon evergreen forests, Science (80-.)., 351(6276), 972–976, doi:10.1126/science.aad5068, 2016.

Wuyts, B., Champneys, A. R. and House, J. I.: Amazonian forest-savanna bistability and human impact, Nat. Commun., 8(May), 1–11, doi:10.1038/ncomms15519, 2017.

Xiao, C. W., Yuste, J. C., Janssens, I. A., Roskams, P., Nachtergale, L., Carrara, A., Sanchez, B. Y. and Ceulemans, R.: Above- and belowground biomass and net primary production in a 73-year-old Scots pine forest, Tree Physiol., 23(8), 505–516, doi:10.1093/treephys/23.8.505, 2003.

Xiao, X., Hagen, S., Zhang, Q., Keller, M. and Moore, B.: Detecting leaf phenology of seasonally moist tropical forests in South America with multi-temporal MODIS images, Remote Sens. Environ., 103(4), 465–473, doi:10.1016/j.rse.2006.04.013, 2006.

Zemp, D. C., Schleussner, C. F., Barbosa, H. M. J., Hirota, M., Montade, V., Sampaio, G., Staal, A., Wang-Erlandsson, L. and Rammig, A.: Self-amplified Amazon forest loss due to vegetation-atmosphere feedbacks, Nat. Commun., 8, 1–10, doi:10.1038/ncomms14681, 2017.
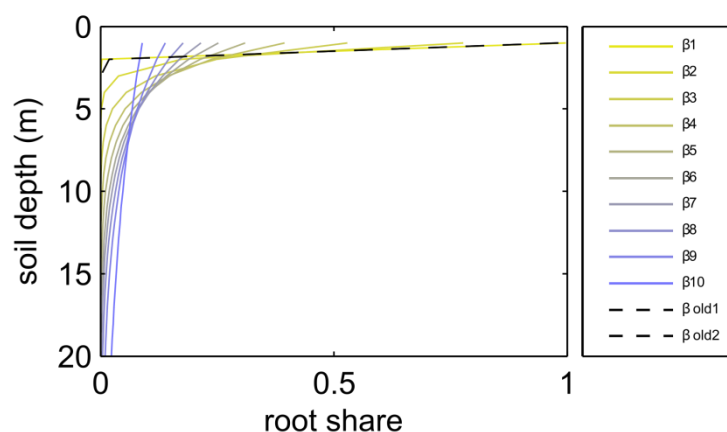
Figure 1: Relative amount of fine roots in each soil layer for different β-values in LPJmL4.0 and LPJmL4.0-VR. In the legend "β old1-2" correspond to the β-values of the 2 tropical tree PFTs (deciduous and evergreen) simulated in LPJmL4.0. The corresponding graphs lie on top of each other due to marginal differences in their β-values. "β1-10" correspond to the 10 β-values used in LPJmL4.0-VR (Table 1) used to create the 10 sub-PFTs of the tropical evergreen and deciduous tree PFTs (Sect. 2.2.3). For LPJmL4.0-VR the fine root distribution at maximum rooting depth is shown. Please note, the first 3 soil layer (as described in 2.2.1) in this visualization are treated as 1 layer of 1 m thickness for reasons of visual clarity.
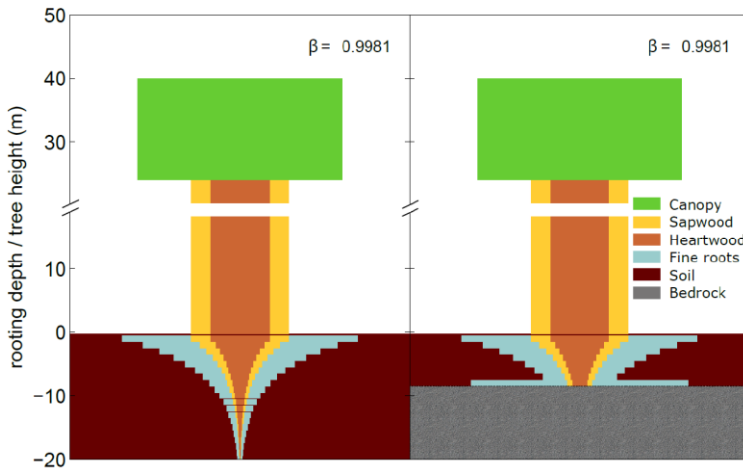
Figure 2: Visualization of belowground carbon allocation to different carbon pools of a tree PFT in LPJmL4.0-VR with a height of 40m and a D_{95_max} of 14m (sub-PFT no. 8 in Table 1) growing in a grid cell with a soil depth of 20m (left panel) and a soil depth of 7m (right panel). As for stem sapwood, also root sapwood needs to satisfy the pipe model. In the first soil layer root sapwood cross-sectional area is equal to stem sapwood cross-sectional area, as all water taken up by fine roots needs to pass this layer. In each following soil layer the root sapwood cross-sectional area is reduced by the sum of the relative amount of fine roots of all soil layers above, thus adjusting the amount of sapwood needed to satisfy the pipe model. Please also see Supplementary Video 1 for a visualization of root growth and development of belowground carbon pools over time under http://www.pik-potsdam.de/~borissa/LPJmL4_VR/Supplementary_Video_1.pptx.
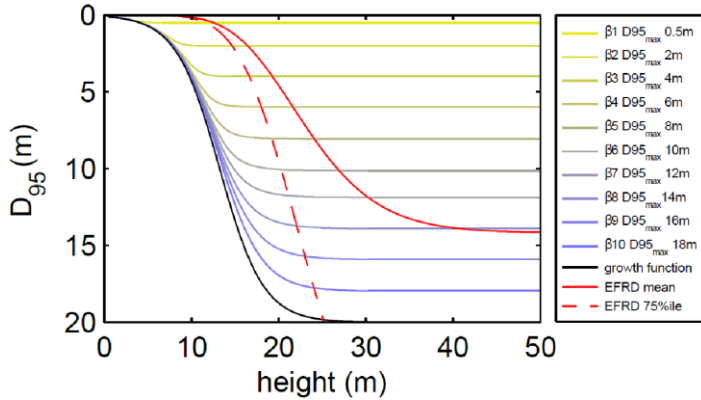

Figure 3: Relation between tree height and rooting depth in LPJmL4.0-VR. Black line: Implemented general growth function of rooting depth (Eq. 5). Lines with colour scale from yellow to blue: Growth functions of rooting depth for each of the 10 sub-PFTs (Sect. 2.2.3). Here temporal rooting depth is expressed as D_{95} and eventually reaches D_{95_max} (Eq. 3). Red solid line: Mean effective functional rooting depth over tree height (EFRD) adapted from Brum *et al.* (2019) using Eq. 5. Red dashed line: Respective 75%ile EFRD over tree height adapted from Brum *et al.* (2019). Please also see Supplementary Video 1 for a visualization of root growth and development of belowground carbon pools over time under http://www.pik-potsdam.de/~borissa/LPJmL4_VR/Supplementary_Video_1.pptx.
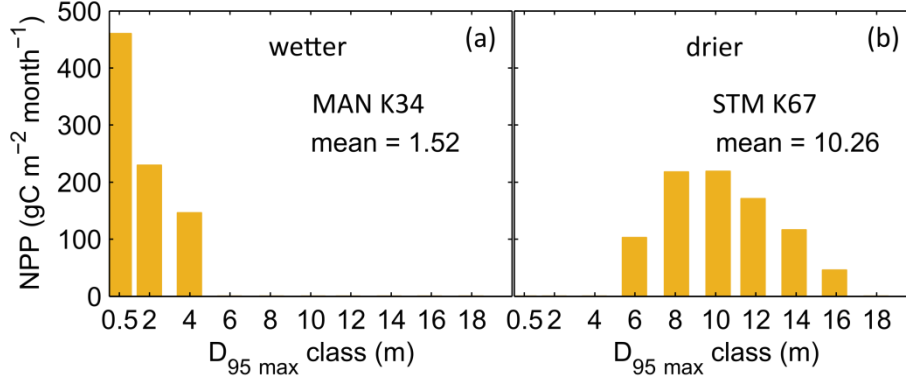
Figure 4: Distributions of simulated mean monthly NPP for each D_{95_max}-class for 2001-2010 under CRU climate input at two FluxNet sites. a) Site MAN K34 near the city of Manaus. b) Site STM K67 near the city of Santarem. For more site information see Table A2 and Fig. 7a.
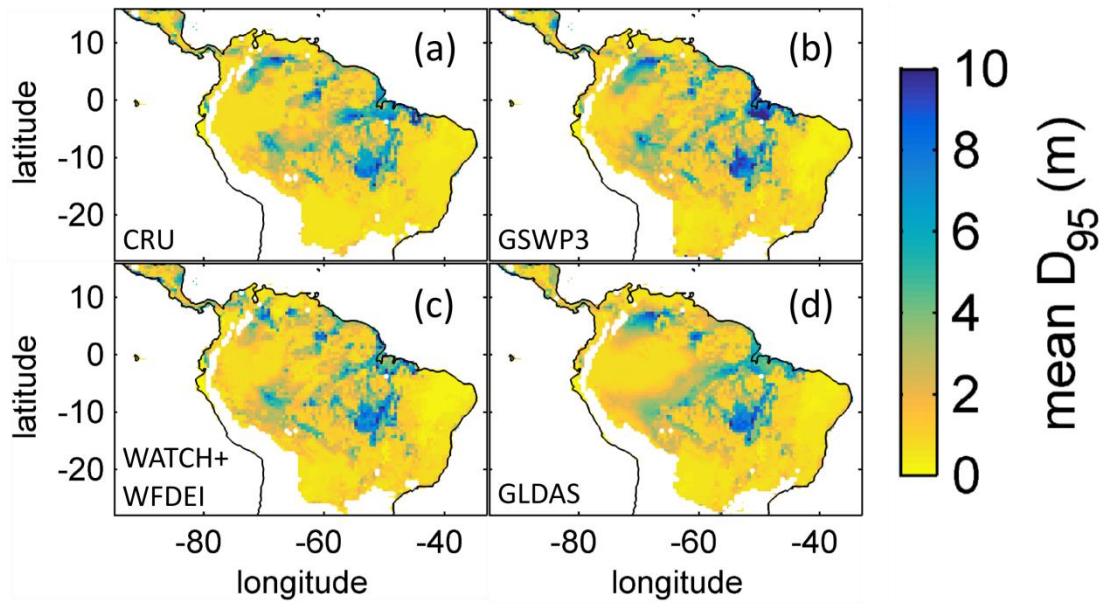
24

Figure 5: Regional NPP-weighted mean rooting depth ($\overline{D_{95}}$) of all sub-PFTs (evergreen and deciduous PFTs combined) for 2001-2010 and different climate inputs simulated with LPJmL4.0-VR. a) CRU climate input. b) GSWP3 climate input. c) WATCH+WFDEI climate input. d) GLDAS climate input. The color scale maximum is set to 10 m.
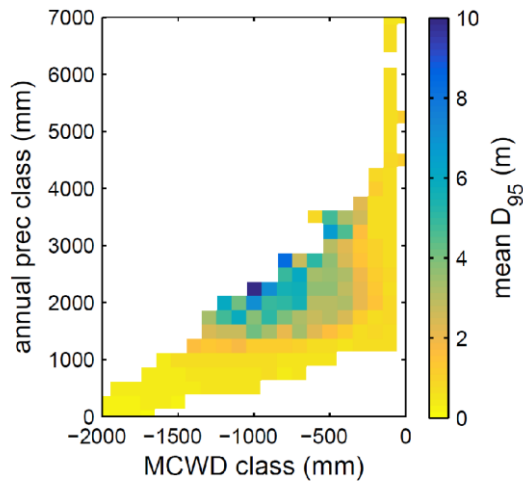

Figure 6: Mean rooting depth depicted as mean $\overline{D_{95}}$ over classes of MCWD and annual precipitation sums. Class step size for precipitation was set to 250 mm and class size for MCWD was set to 50 mm. Regions with high amounts of annual rainfall and lower seasonality exclusively favour shallow rooted forests (low $\overline{D_{95}}$). $\overline{D_{95}}$ increases with decreasing MCWD (increasing seasonal drought stress) and decreasing sums of annual precipitation. Below 1200 mm of annual rainfall or -1100 mm of MCWD $\overline{D_{95}}$ sharply decreases again. Note this figure does not consider soil depth. The color scale maximum is set to 10 m.
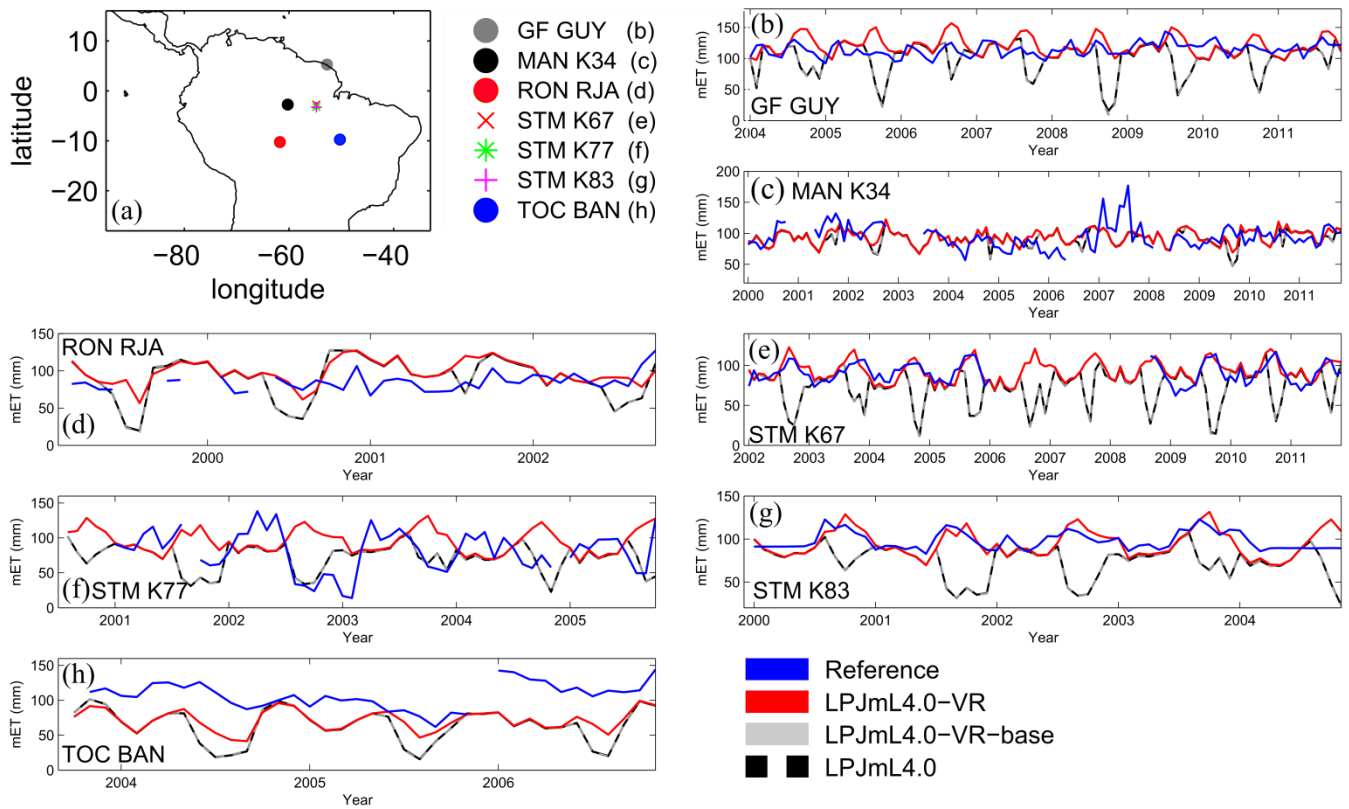
Figure 7: Comparisons of monthly ET between different Fluxnet sites and respective simulation output of the different LPJmL model versions used in this study forced with CRU climate. a) Geographical location of different Fluxnet sites (see also Table A2). For statistical measures of the individual comparison see Table A3.
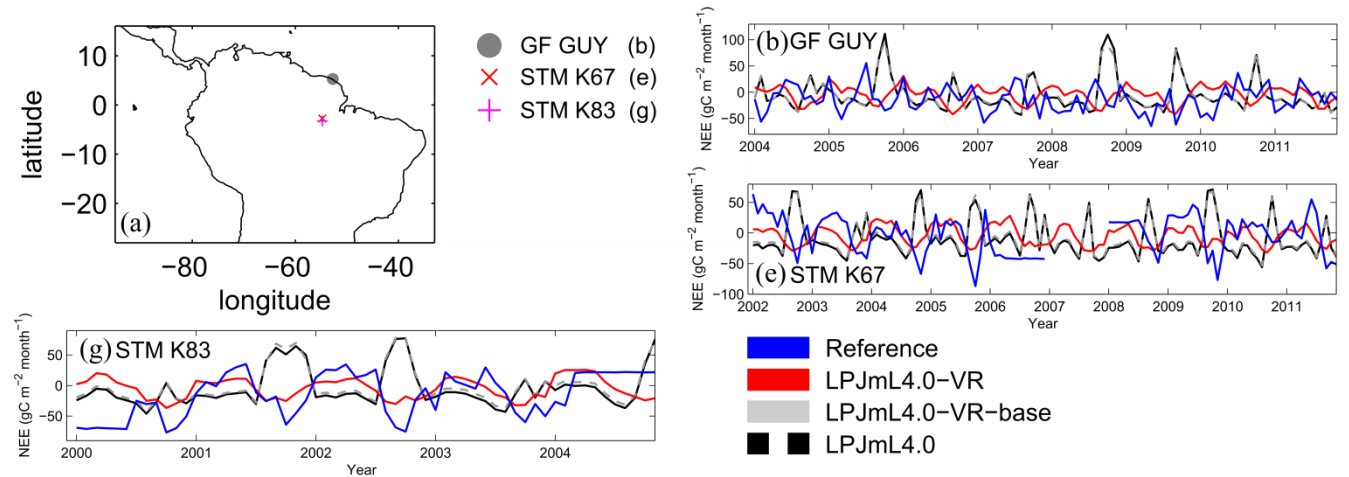

Figure 8: Comparisons of monthly NEE between different Fluxnet sites and respective simulation output of the different LPJmL model versions used in this study forced with CRU climate. a) Geographical location of different Fluxnet sites (see also Table A2). For statistical measures of the individual comparison see Table A4. Note due to data scarcity only 3 Fluxnet sites are shown. Plots of all sites are shown in Fig. A5. We kept panel labelling as in Fig. 7 to ensure easy comparability.
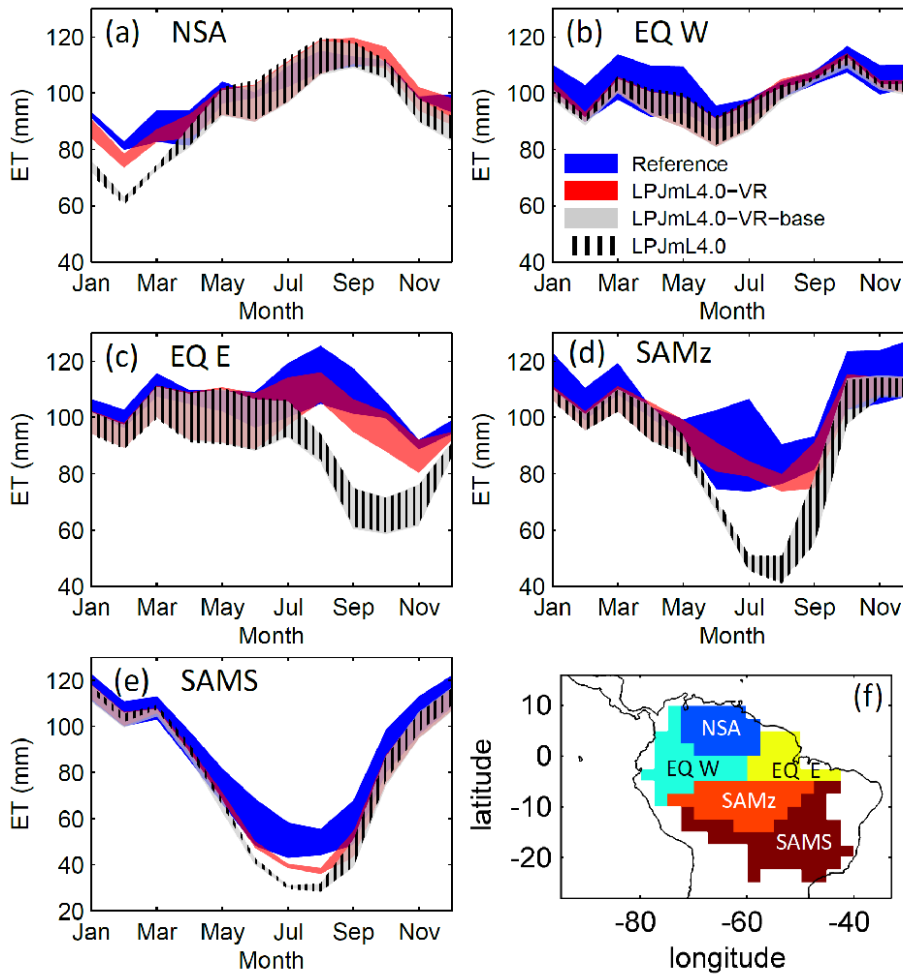
Figure 9: Comparisons of continental scale gridded ET products against simulated ET within 5 regional climatological clusters (a-e) as defined in Sect. 2.5.1. Shown is the mean annual cycle of 1981-2010 and the mean for the whole cluster area. Corridors denote the minimum-maximum range between either the ET products or the model outputs under the different climate forcings used in this study. f) Geographical extent of climatological clusters (adapted from Sörensson and Ruscica, 2018). Statistical measures of the individual comparisons can be found in Table A5 (comparisons of corridor means).
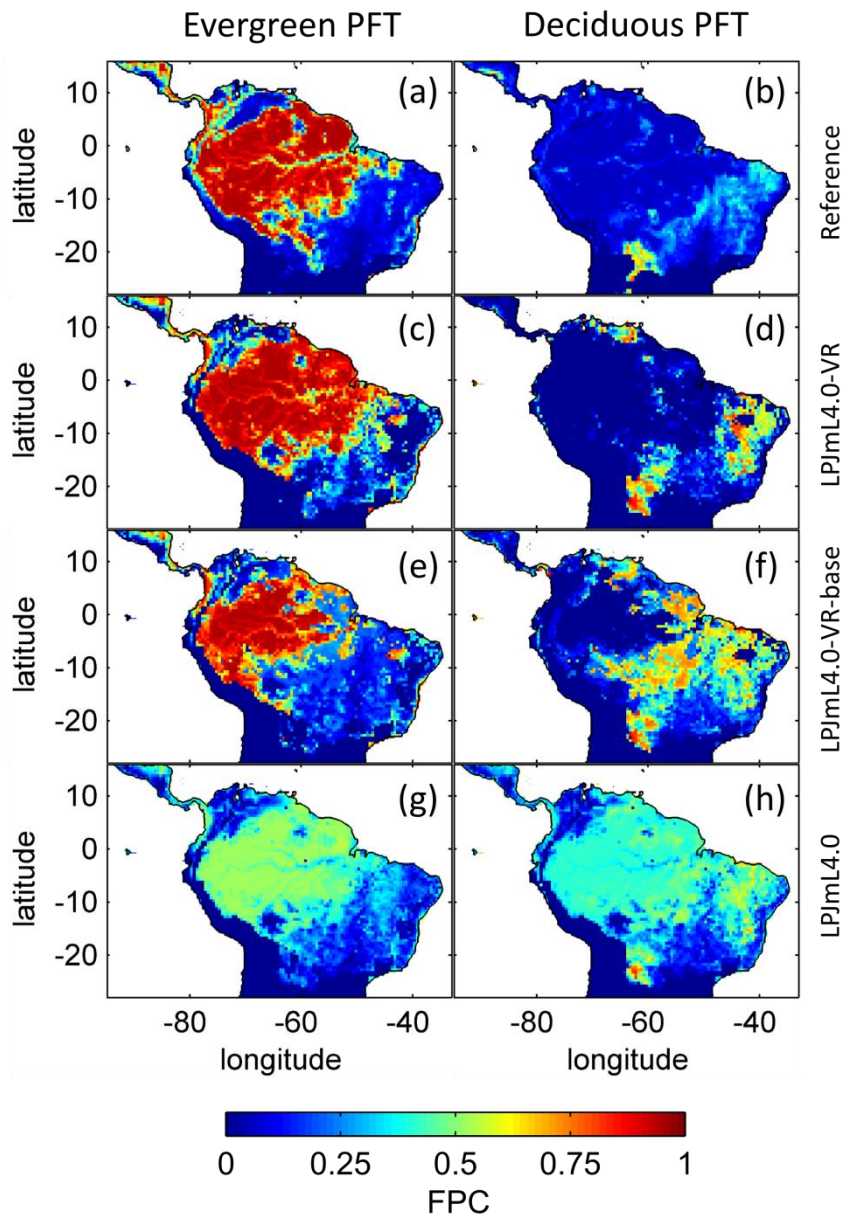
Fig. 10: Foliage projected cover (FPC) of evergreen (a, c, e, g) and deciduous (b, d, f, h) PFTs over the study region. a)-b) Satellite-derived vegetation composition from ESA Land cover CCI V2.0.7 (Li et al., 2018) **reclassified to the PFTs of LPJmL as in** (Forkel et al., 2014)**. b)-c) LPJmL4.0-VR. d)-e) LPJmL4.0-VR-base. f)-g) LPJmL4.0. All LPJmL model versions were forced with CRU climate input. The shown FPC for all models refers to 2001-2010. For statistical measures of individual comparisons between model versions (c-h) and satellite derived vegetation composition (a-b) see Table A6.**
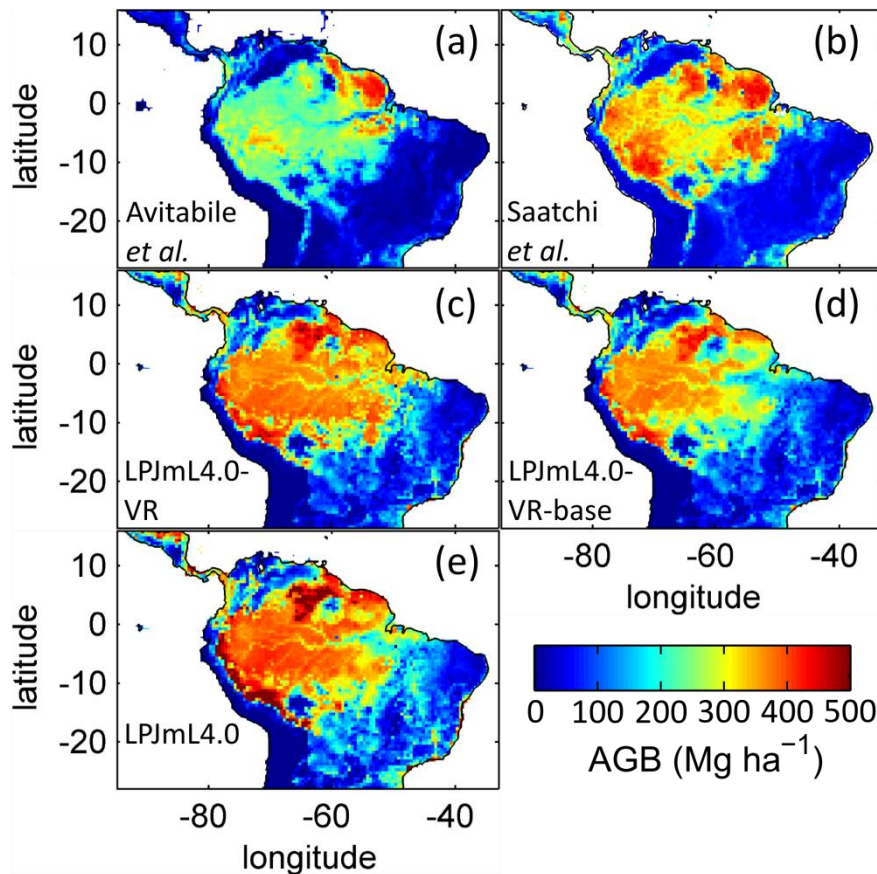
28

Fig. 11: Comparison of simulated AGB and satellite derived AGB validation products regridded to the spatial resolution of LPJmL models. a) Biomass validation product from Avitabile *et al.* (2016b). b) AGB validation product from Saatchi *et al.*, (2011). c)-e) Mean AGB simulated for the time span 2001-2010 with c) LPJmL4.0-VR. d) LPJmL4.0-VR-base and e) LPJmL4.0. For statistical measures of individual comparisons between model versions (c-e) and satellite derived AGB evaluation products (a-b) see Table A7.
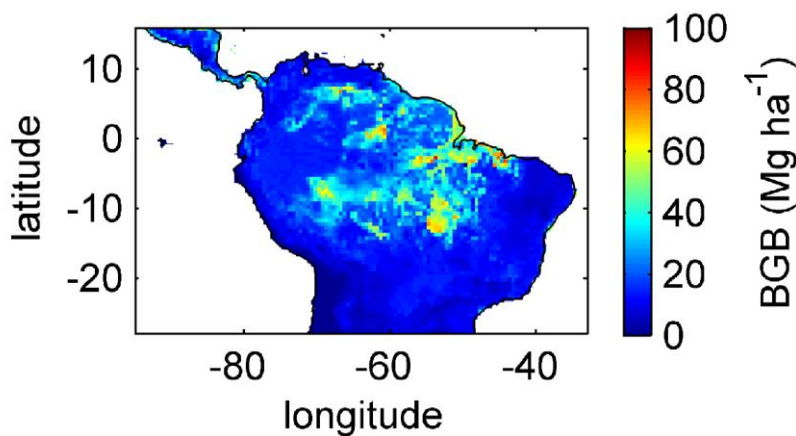

Fig. 12: Mean sum (2001-2010) of belowground biomass (BGB; sum of tree coarse and fine roots) of evergreen and deciduous tree PFTs simulated with LPJmL4.0-VR under CRU climate forcing.
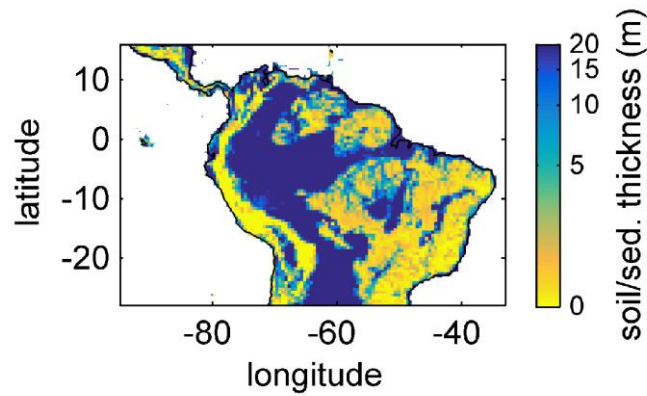
Table 1: β-values assigned to the 10 sub-PFTs of each tropical PFT (evergreen and deciduous) in LPJmL4.0-VR and the corresponding maximum rooting depth reached by 95% of the roots (D_{95_max}).

sub-PFT number	β-value	D_{95_max} (m)
1	0.9418	0.5
2	0.9851	2
3	0.9925	4
4	0.995	6

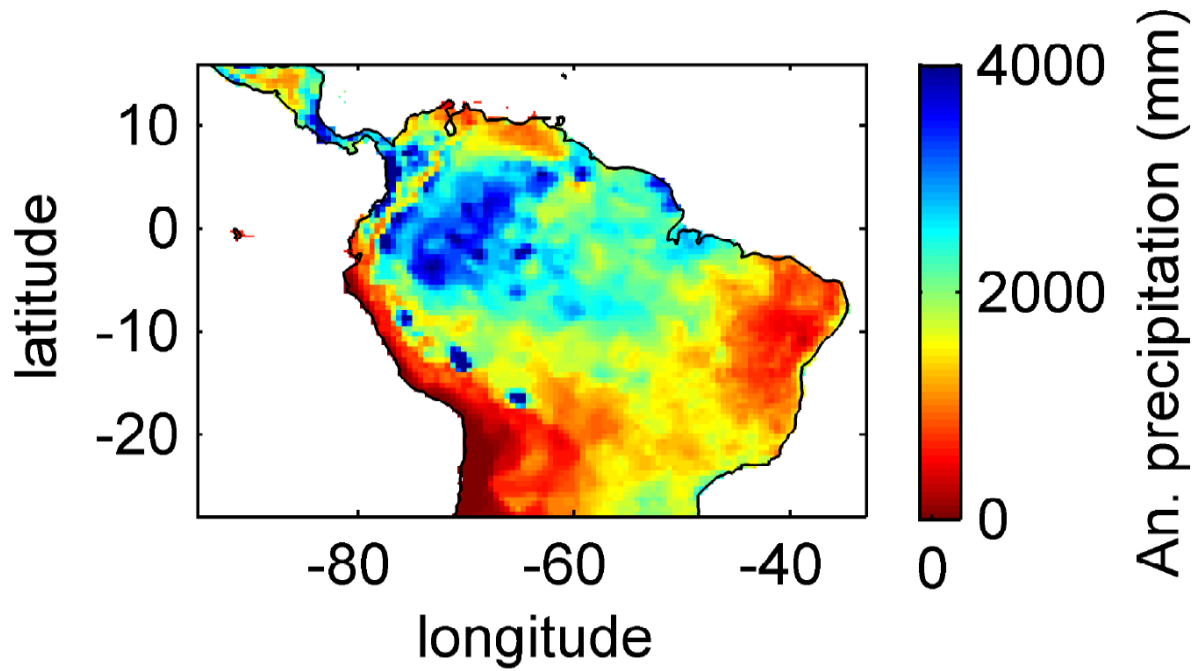|		
5	0.9963	8
6	0.9971	10
7	0.9976	12
8	0.9981	14
9	0.9986	16
10	0.9993	18

994

995 **12 Appendix A**

996
997 **Figure A1: Soil/sediment thickness from** (Pelletier et al., 2016) **regridded to the 0.5° x 0.5° longitude-latitude grid of LPJmL4.0-VR**
998 **and restricted to a maximum of 20 m. Colorbar in decadic logarithm.**

999
1000 **Figure A2: Mean annual precipitation for 2001-2010 under CRU climate input.**
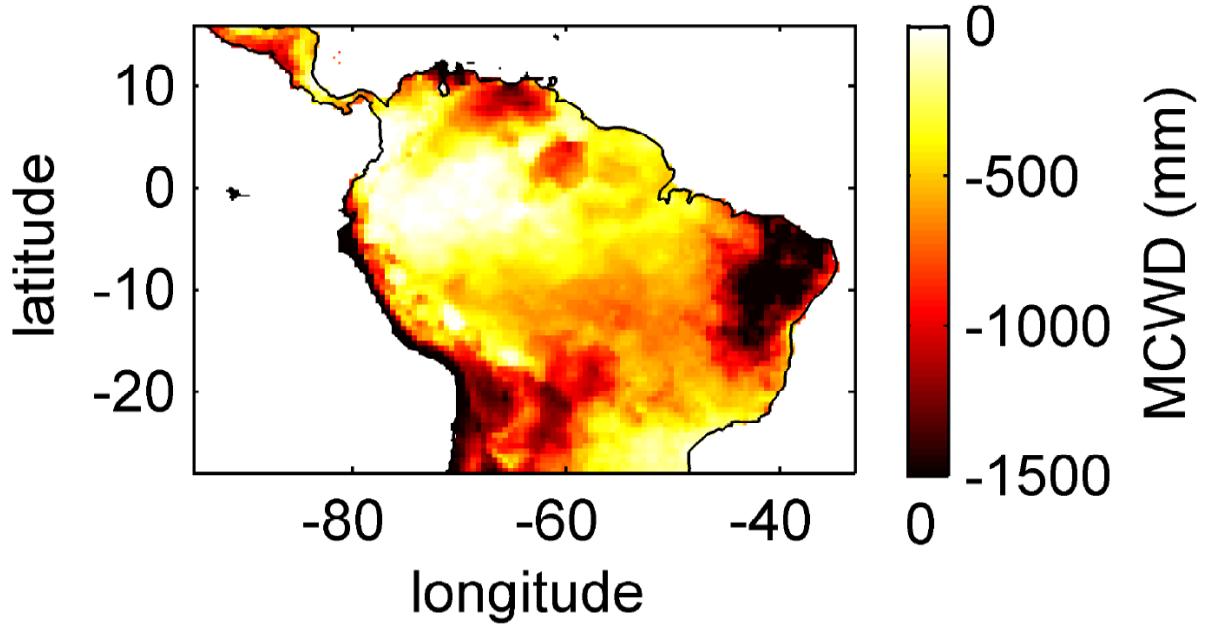
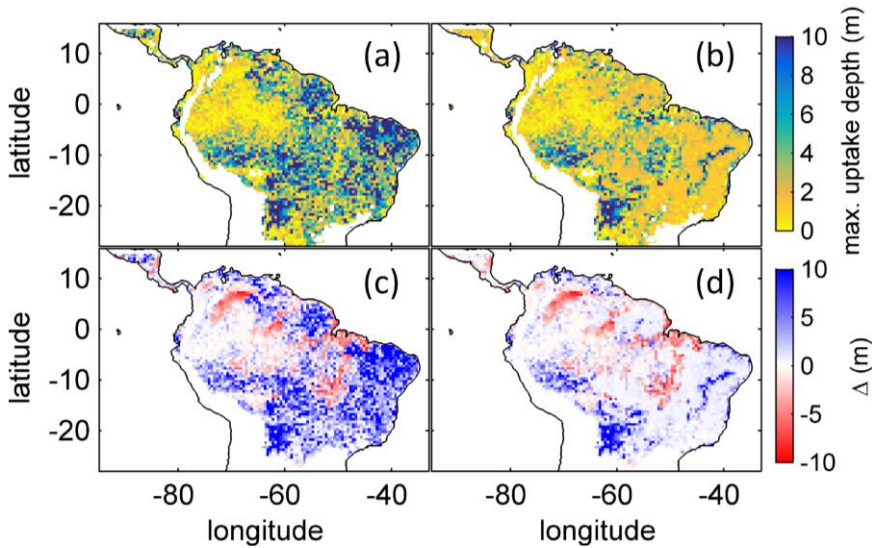Figure A3: Mean annual MCWD for 2001-2010 under CRU climate input.

Figure A4: Comparison of simulated $\overline{D_{95}}$ to product of maximum tree root water uptake depth (MDRU). a) Original (Fan et al., 2017) MDRU regridded to 0.5°x0.5° resolution of LPJmL4.0-VR. b) Same as a) but adjusted to soil depth input used in this study (see 2.3.2), in cases where values of (Fan et al., 2017) exceeded this soil depth. The color scale maximum for a) and b) is set to 10 m. c) Difference between a) and $\overline{D_{95}}$ simulated with LPJmL4.0-VR under CRU climate forcing (Fig. 6a). d) Difference between b) and $\overline{D_{95}}$ simulated with LPJmL4.0-VR under CRU climate forcing (Fig. 5a). Red/blue colors denote higher/lower rooting depths in LPJmL4.0-VR.
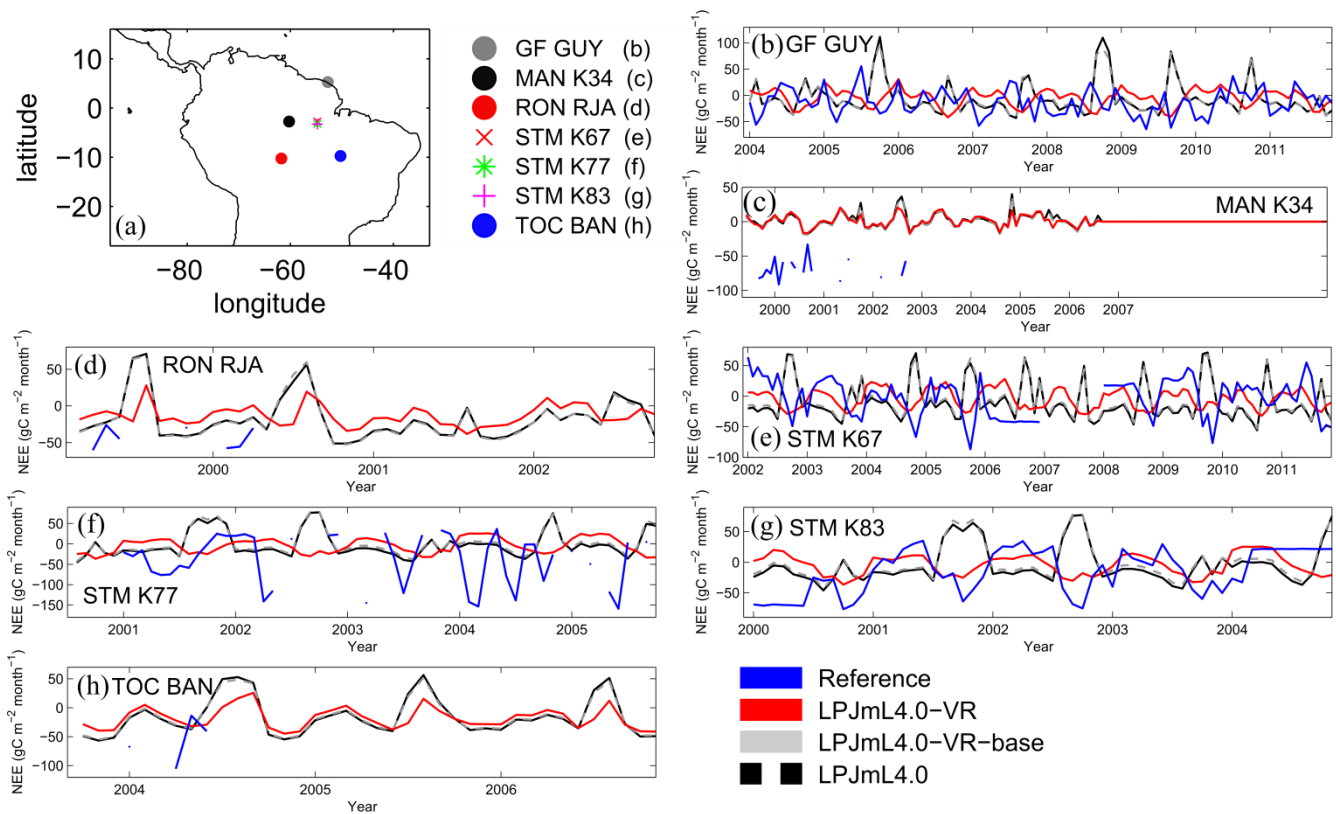
Fig. A5: Comparisons of monthly NEE between different Fluxnet sites and respective simulation output of the different LPJmL model versions used in this study forced with CRU climate. a) Geographical location of different Fluxnet sites (see also Table A2).

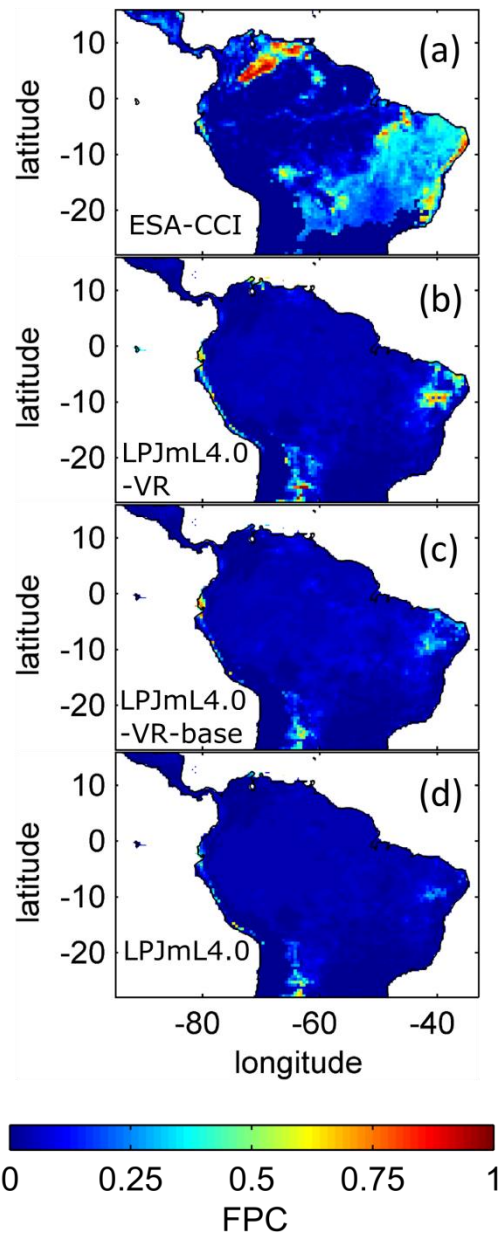Figure A6: Foliage projected cover (FPC) of the tropical herbaceous PFT over the study region. a) Satellite-derived vegetation composition from ESA Land cover CCI V2.0.7 (Li et al., 2018) reclassified to the PFTs of LPJmL as in (Forkel et al., 2014). b) LPJmL4.0-VR. c) LPJmL4.0-VR-base. d) LPJmL4.0. All LPJmL model versions were forced with CRU climate input. The shown FPC for all models refers to 2001-2010.
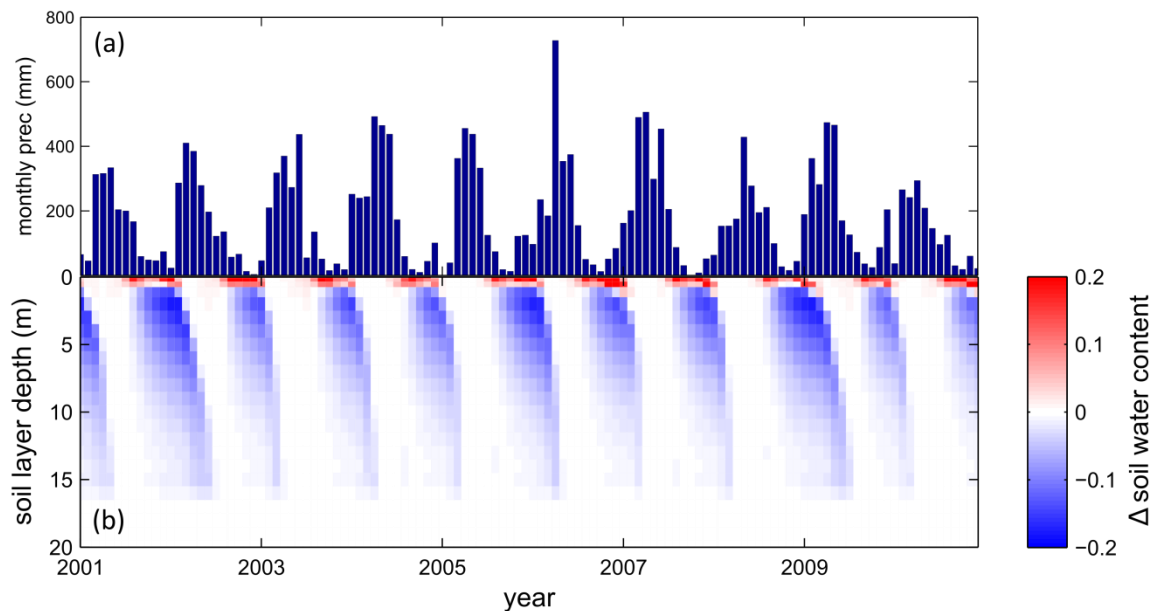
Figure A7: Difference in soil water reaction to seasonal precipitation between LPJmL4.0-VR-base and LPJmL4.0-VR at Fluxnet site STM KM67 a) Mean monthly precipitation input from CRU for 2001-2010. b) Difference in monthly relative soil water content between LPJmL4.0-VR-base and LPJmL4.0-VR forced with CRU climate for 2001-2010. The underlying model output variable "soil water content" of each model version is a number between 0 and 1 depicting the relative water saturation of the soil. Blue colors denote lower soil water content in LPJmL4.0-VR and red colors a lower soil water content in LPJmL4.0-VR-base.

Table A1: Soil layer partitioning scheme used in LPJmL4.0-VR. The first meter of the soil column is split into 3 soil layers and after 1m of soil depth each following soil layer is assigned a thickness of 1 m as in LPJmL4.0. Whereas LPJmL4.0's last soil layer reaches 3 m, LPJmL4.0-VR's last soil layer reaches 20 m.

Soil layer number	Soil layer boundary (m)	Soil layer thickness (m)
1	0.2	0.2
2	0.5	0.3
3	1	0.5
4	2	1
…	…	…
23	20	1

Table A2: Description of Fluxnet sites used for the evaluation of simulated ET.

Site name	Short name	Country	LPJmL coordinate latitude	longitude
Ecotone Bananal Island/BR-Ban	TOC_BAN	Brazil	-9.75	-50.25
Manaus-ZF2 K34/BR-Ma2	MAN_K34	Brazil	-2.75	-60.25
Santarem-Km67-Primary Forest/BR-Sa1	STM_K67	Brazil	-2.75	-54.75
Santarem-Km77-Pasture/BR-Sa2	STM_K77	Brazil	-3.25	-54.75
Santarem-Km83-Logged Forest/BR-Sa3	STM_K83	Brazil	-3.25	-54.75
Rond.- Rebio Jaru Ji Parana-Tower B/BR-Ji3	RON_RJA	Brazil	-10.25	-61.75
Guyaflux	GF_GUY	French Guiana	5.25	-52.75

34

1032

1033 **Table A3: Normalized mean error (NME), coefficient of determination (r²) and p-value of F-statistic piecewise calculated for**
1034 **simulated ET of the different LPJmL model versions used in this study forced with CRU climate input and Fluxnet data of ET at 7**
1035 **Fluxnet sites (in accordance with Fig. 7).**

Statistic	Model	TOC_BAN	MAN_K34	STM_K67	STM_K77	STM_K83	RON_RJA	GF_GUY
NME	LPJmL4.0-VR	2.41	1.11	0.75	1.38	1.10	2.28	1.57
	LPJmL4.0-VR-base	2.92	1.22	2.29	0.98	2.74	2.73	2.38
	LPJmL4.0	2.93	1.23	2.27	0.98	2.74	2.70	2.36
r²	LPJmL4.0-VR	0.09	0.03	0.53	0.17	0.43	0.01	0.08
	LPJmL4.0-VR-base	0.10	0.00	0.33	0.14	0.03	0.01	0.01
	LPJmL4.0	0.09	0.00	0.33	0.14	0.03	0.01	0.01
p-value	LPJmL4.0-VR	0.075	0.041	< 0.001	0.002	< 0.001	0.575	0.005
	LPJmL4.0-VR-base	0.067	0.585	< 0.001	0.005	0.221	0.517	0.277
	LPJmL4.0	0.068	0.672	< 0.001	0.005	0.221	0.514	0.274

1036

1037 **Table A4: Normalized mean error (NME), coefficient of determination (r²) and p-value of F-statistic piecewise calculated for**
1038 **simulated NEE of the different LPJmL model versions used in this study forced with CRU climate input and Fluxnet data of NEE**
1039 **at 3 Fluxnet sites (in accordance with Fig. 8).**

Statistic	Model	STM_K67	STM_K83	GF_GUY
NME	LPJmL4.0-VR	0.90	0.84	1.30
	LPJmL4.0-VR-base	1.62	1.36	1.52
	LPJmL4.0	1.68	1.39	1.52
r²	LPJmL4.0-VR	0.16	0.14	0.00
	LPJmL4.0-VR-base	0.32	0.06	0.03
	LPJmL4.0	0.33	0.07	0.03
p-value	LPJmL4.0-VR	< 0.001	0.003	0.515
	LPJmL4.0-VR-base	< 0.001	0.055	0.046
	LPJmL4.0	< 0.001	0.047	0.059

1040

1041 **Table A5: Normalized mean error (NME), coefficient of determination (r²) and p-value of F-statistic piecewise calculated for the**
1042 **simulated ET of the different LPJmL model versions used in this study and continental scale gridded ET products within 5**
1043 **regional climatological clusters. With respect to Fig. 9 comparisons are based on the monthly mean of corridors shown, i.e. 1) the**
1044 **monthly mean of all outputs produced by one LPJmL model version but forced with different climate inputs and 2) the monthly**
1045 **mean of all continental scale gridded ET data products.**

Statistic	Model	NSA	EQ W	EQ E	SAmz	SAMS
NME	LPJmL4.0-VR	0.08	0.26	0.62	0.20	0.06
	LPJmL4.0-VR-base	0.37	0.42	1.95	0.58	0.13
	LPJmL4.0	0.34	0.26	1.92	0.58	0.11
r²	LPJmL4.0-VR	0.98	0.94	0.91	0.98	1.00
	LPJmL4.0-VR-base	0.94	0.96	0.20	0.91	0.99
	LPJmL4.0	0.93	0.96	0.21	0.90	0.99
p-value	LPJmL4.0-VR	< 0.001	< 0.001	< 0.001	< 0.001	< 0.001
	LPJmL4.0-VR-base	< 0.001	< 0.001	0.143	< 0.001	< 0.001
	LPJmL4.0	< 0.001	< 0.001	0.135	< 0.001	< 0.001

1046

1047 **Table A6: Normalized mean error (NME) of FPC comparison piecewise calculated between 1) the satellite-derived vegetation**
1048 **composition from ESA Land cover CCI V2.0.7 (Li et al., 2018) reclassified to the PFTs of LPJmL as in Forkel et al. (2014) and 2)**
1049 **all LPJmL model versions used in this study forced with CRU climate data (in accordance with Fig. 10).**

Statistic	Model	FPC Evergreen	FPC Deciduous
NME	LPJmL4.0-VR	0.31	1.01
	LPJmL4.0-VR-base	0.38	1.5
	LPJmL4.0	0.47	1.76

1050

1051 **Table A7: Normalized mean error (NME) of AGB comparison piecewise calculated between 1) the satellite-derived AGB**
1052 **validation products and 2) all LPJmL model versions used in this study forced with CRU climate data (in accordance with Fig. 11).**

Statistic	Model	Avitabile *et al.*	Saatchi *et al.*

NME	LPJmL4.0-VR	0.78	0.12
	LPJmL4.0-VR-base	0.69	0.11
	LPJmL4.0	1.09	0.14

1053